

VILNIUS UNIVERSITY  
CENTER FOR PHYSICAL SCIENCES AND TECHNOLOGY

ALBERTAS ŽUKAUSKAS

**FABRICATION OF OPTICAL COMPONENTS FOR LIGHT  
CONTROL AT MICROMETER SCALE BY DIRECT LASER  
WRITING**

Summary of doctoral dissertation  
Technological Sciences, Materials Engineering (08T)

Vilnius, 2015

---

The doctoral dissertation was prepared during 2011 – 2015 at Vilnius University.

**Scientific supervisor** – prof. dr. Roaldas Gadonas (Vilnius University, Technological Sciences, Materials Engineering – 08T).

**Doctoral committee:**

**Chairman** – prof. habil. dr. Valdas Sirutkaitis (Vilnius University, Technological Sciences, Materials Engineering – 08T).

**Members:**

- dr. Martynas Beresna (University of Southampton, United Kingdom, Technological Sciences, Materials Engineering – 08T);
- prof. habil. dr. Juozas Vidas Gražulevičius (Kaunas University of Technology, Technological Sciences, Materials Engineering – 08T);
- dr. Gediminas Račiukaitis (Center for Physical Sciences and Technology, Technological Sciences, Materials Engineering – 08T);
- dr. Bonifacas Vengalis (Center for Physical Sciences and Technology, Technological Sciences, Materials Engineering – 08T).

The dissertation will be defended under open consideration in the Council of Materials Science on the 18th of December, 2015, 15:00 h at the Laser Research Center of Vilnius University, room 306, Saulėtekio Ave. 10, Vilnius, Lithuania.

The summary of the dissertation was distributed on the 18th of November, 2015.

The dissertation is available at Vilnius University, Center for Physical Sciences and Technology libraries, and VU website [www.vu.lt/lt/naujienos/ivykiu-kalendorius](http://www.vu.lt/lt/naujienos/ivykiu-kalendorius).

VILNIAUS UNIVERSITETAS  
FIZINIŲ IR TECHNOLOGIJOS MOKSLŲ CENTRAS

ALBERTAS ŽUKAUSKAS

**OPTINIŲ ELEMENTŲ ŠVIESOS VALDYMUI MIKROMETRINIAME  
MASTELYJE FORMAVIMAS TIESIOGINIO LAZERINIO RAŠYMO  
BŪDU**

Daktaro disertacija  
Technologijos mokslai, medžiagų inžinerija (08T)

Vilnius, 2015

---

Disertacija rengta 2011 – 2015 metais Vilniaus universitete.

**Mokslinis vadovas** – prof. dr. Roaldas Gadonas (Vilniaus universitetas, technologijos mokslai, medžiagų inžinerija – 08T).

**Disertacija ginama Vilniaus universiteto medžiagų inžinerijos mokslų krypties taryboje:**

**Pirmininkas** – prof. habil. dr. Valdas Sirutkaitis (Vilniaus universitetas, technologijos mokslai, medžiagų inžinerija – 08T).

**Nariai:**

- dr. Martynas Beresna (Southamptono universitetas, Jungtinė Karalystė, technologijos mokslai, medžiagų inžinerija – 08T);
- prof. habil. dr. Juozas Vidas Gražulevičius (Kauno technologijos universitetas, technologijos mokslai, medžiagų inžinerija – 08T);
- dr. Gediminas Račiukaitis (Fizinių ir technologijos mokslų centras, technologijos mokslai, medžiagų inžinerija – 08T);
- dr. Bonifacas Vengalis (Fizinių ir technologijos mokslų centras, technologijos mokslai, medžiagų inžinerija – 08T).

Disertacija bus ginama viešame Medžiagų inžinerijos mokslo krypties tarybos posėdyje 2015 m. gruodžio 18 d. 15:00 val. Vilniaus universiteto lazerinių tyrimų centro 306 auditorijoje, Saulėtekio al. 10, Vilniuje, Lietuvoje.

Disertacijos santrauka išsiuntinėta 2015 m. lapkričio 18 d.

Disertaciją galima peržiūrėti Vilniaus universiteto, Fizinių ir technologijos mokslų centro bibliotekose ir VU interneto svetainėje adresu [www.vu.lt/lt/naujienos/ivykiu-kalendorius](http://www.vu.lt/lt/naujienos/ivykiu-kalendorius).

---

## Table of Contents

---

<b>Introduction</b>	<b>6</b>
Subject and Scope of the Thesis . . . . .	7
Novelty . . . . .	7
Practical Value . . . . .	7
Statements to Defend . . . . .	8
Approbation . . . . .	8
Contribution of the Authors . . . . .	12
Structure of the Thesis . . . . .	13
<b>1 Review of the Literature</b>	<b>14</b>
1.1 Microoptical elements: history, classification and fabrication methods	14
1.2 Direct laser writing technique: principles and applications . . . . .	16
<b>2 Experimental Methods</b>	<b>18</b>
<b>3 Investigation of the Polymers' Optical Resistance</b>	<b>21</b>
3.1 Spectrophotometric characterization results . . . . .	21
3.2 Nano- and femtosecond pulses induced damage of the SZ2080 . . . . .	22
3.3 Laser-induced damage threshold of other polymers . . . . .	23
<b>4 Singular Optical Components</b>	<b>26</b>
4.1 Fabrication of the microoptical components . . . . .	26
4.2 Conical microlenses . . . . .	27
4.3 Spiral phase plates . . . . .	28
4.4 Bifunctional optical elements . . . . .	29
4.5 Fabrication of complex microoptical elements on fiber tip . . . . .	30
<b>5 Optical Components with Gradient Refractive Index</b>	<b>32</b>
5.1 Change in chemical properties under light exposure . . . . .	32
5.2 Tailoring of the refractive index . . . . .	34
<b>Conclusions</b>	<b>36</b>
<b>Bibliography</b>	<b>37</b>
<b>Santrauka</b>	<b>43</b>
<b>Curriculum vitae</b>	<b>45</b>

---

## Introduction

---

Miniaturization of devices and increase in their functionality is a common trend of nowadays technologies over all areas. A simple example from daily life is video and audio compact discs. An in-depth examination of their evolution reveals several tendencies: geometric dimensions decrease, and the amount of data increases. It is an example of rapid miniaturization processes and functionality improvement driven by economic, technological and environmental aspects. The rate of this processes is clearly seen in semiconductors' industry: Moore's law claims that the number of transistors in a dense integrated electronic circuit doubles every two years. The same progression is prominent in the fabrication of medical, mechanical, microfluidic, and finally – optical devices. Since the 8th decade of the 20th century the trend of miniaturization of optical devices gradually moved from scientific laboratories (principal demonstrations) to industry (real-life applications and mass production). Its great success was determined by an adoption of numerous fabrication techniques, MOCs' functionality, integrity, longevity, sufficiently small scale and reasonable costs. The progress of the MOCs formation was continuously stimulated by the demand to control the light propagation at the micrometer scale. It requires the dedicated tools – aforementioned microoptical elements, which can be defined as follows:

*Microoptical components are optical elements that are between a few micrometers and a millimeter in size.*

The scientific interest in the field of microoptics is growing rapidly although this branch of science exists for only more than a couple of decades with practical applications keeping in step. At the moment, microoptical elements are used in *Shack Hartmann* sensors, lightning systems, light emitting diodes, laser micromachining and medicine [1]. As a result, the demand for the MOCs is continuously growing and the desire to create innovative optical elements with novel functionality arises. Yet, not everything can be done with the classical cutting, grinding and polishing techniques, but the technologies evolve and make it possible to realize new ideas. One of such technologies is a direct laser writing (DLW) technique based on non-linear interaction between laser irradiation and light sensitive materials (prepolymers) [2]. This technology, introduced almost two decades ago in 1997, offers unique possibilities for fabricating three-dimensional (3D) microstructures in a single step with lateral and axial resolutions beyond the diffraction limit. Later, it has also found applications in the field of microoptics [3]. Up to now, numerous scientific articles have appeared in literature on the manufacturing of classical minimized optical elements, analysis of the DLW experimental parameters, process performance optimization and various aspects of the applications. Despite to noticeable progress in this field, we are going

to focus on the fabrication of singular microoptical elements and extend the range of DLW possible applications. Moreover, we are going to reveal the potential to manufacture structures with the imprinted spatial refractive index distribution which has not been reported so far in the growing field of direct laser writing. Finally, we shift the focus to determination and characterization of polymers' optical properties which can be a limiting factor for further applications of the microoptical elements produced by DLW.

## **Subject and Scope of the Thesis**

The aim of this work is to investigate the experimental possibility to manufacture singular and gradient refractive index microoptical elements via direct laser writing technique out of hybrid organic-inorganic prepolymer and to employ these components for the light flow control at the micrometer scale. In addition, it is aimed to characterize optical and chemical properties of the hybrid polymer used within this work.

## **Novelty**

1. Spectrophotometric properties (transmittance, absorption coefficient, complex refractive index) of the hybrid organic-inorganic polymer SZ2080 was determined in a 230–1000 nm spectral range.
2. The optical resistance of the various polymers used in DLW technique is determined by means of laser-induced damage threshold evaluation according to an ISO certified testing method.
3. Fabrication of different geometry singular microoptical components using direct laser writing technique is demonstrated. The propagation of the light through the manufactured elements is investigated.
4. For the first time, the suitability of the direct laser writing technology for the fabrication of gradient-index microoptical elements with the largest refractive index change of the order of  $10^{-2}$  is demonstrated. The relationship between the refractive index and degree of conversion and its dependence on the exposure dosage to the laser radiation is determined.

## **Practical Value**

The practical value of this work is reflected by the possibility to shape the light flow at the micrometer scale both with different geometry and gradient refractive index microoptical elements manufactured via direct laser writing technique out of light sensitive prepolymers. The main advantages of these components are:

1. Laser-induced damage threshold of polymers is comparable with the optical resistance of the anti-reflective coatings.
2. Polymers are transparent materials in the visible and near-infrared spectral range.

3. The surface roughness of the fabricated components is limited by the material properties itself and is smaller than  $\lambda/10$  in the visible spectral range.
4. It is possible to induce refractive index change of the order of  $10^{-2}$  within single fabricated microstructure.
5. DLW fabrication technique is simple and promising. Also it is in a continual improvement process for various applications.
6. The geometric shape of the microoptical elements is chosen freely and asymmetric microstructures can be produced.
7. Complex optical systems consisting of numerous elements can be simplified by the use of a single monolithic multifunctional microoptical component.
8. Microoptical elements can be manufactured not only on a standard glass substrates, but integrated into more complex systems or production stages as well.

In regard to the aforementioned properties, microoptical elements, fabricated by the means of DLW technique, may pave the way for practical applications in laser micromachining, optical tweezers, sensors, etc.

### Statements to Defend

1. Optical resistance of the hybrid polymer SZ2080, used for the manufacturing of microoptical components via direct laser writing technique, is comparable with the materials', widely used for the anti-reflective coatings, at nanosecond pulse duration testing regime ( $f = 50$  Hz,  $\tau = 11$  ns and 6.2 ns,  $\lambda = 1064$  nm and 532 nm). Meanwhile, at femtosecond pulse duration testing regime ( $f = 50$  kHz,  $\tau = 343$  fs,  $\lambda = 1030$  nm and 515 nm) optical resistance is in 0.1–0.6 J/cm<sup>2</sup> range.
2. It is possible to fabricate functional singular microoptical elements via direct laser writing technique out of hybrid prepolymer SZ2080 using concentric ring and spiral laser beam scanning algorithms with decreasing radius. Light beams propagating through the fabricated elements are distinguished by the optical vortexes' and zero and higher-order Gaussian and Bessel beams' properties: annular intensity distribution, propagation invariability in near field and zero intensity at the central part of the beam.
3. The variation of the exposure dose during direct laser writing process leads to the alteration of the consumed double carbon-carbon bonds during the radical polymerization reaction in SZ2080 prepolymer. It allows to control the refractive index from  $1.501 \pm 0.001$  to  $1.516 \pm 0.001$  and to induce desired distribution of the refractive index in a fabricating structure.

### Approbation

*Scientific articles in the periodical journals with an impact factor which are included in the database of Institute for Scientific Information (ISI).*



- [A1] E. Brasselet, M. Malinauskas, **A. Žukauskas** and S. Juodkazis, Photopolymerized microscopic vortex beam generators: Precise delivery of optical orbital angular momentum, *Appl. Phys. Lett.* **97**, 211108 (2010).
- [A2] **A. Žukauskas**, M. Malinauskas, C. Reinhardt, B.N. Chichkov, and R. Gadonas, Closely packed hexagonal conical microlens array fabricated by laser photopolymerization, *Appl. Opt.* **51**(21), 4995–5003 (2012).
- [A3] M. Malinauskas, **A. Žukauskas**, V. Purlys, A. Gaidukevičiūtė, Z. Balevičius, A. Piskarskas, C. Fotakis, S. Pissadakis, D. Gray, R. Gadonas, M. Vamvakaki, and M. Farsari, 3D microoptical elements formed in a photostructurable germanium silicate by direct laser writing, *Opt. Laser. Eng.* **50**(12), 1785–1788 (2012).
- [A4] **A. Žukauskas**, M. Malinauskas, and E. Brasselet, Monolithic generators of pseudo-nondiffracting optical vortex beams at the microscale, *Appl. Phys. Lett.* **103**, 181122 (2013).
- [A5] **A. Žukauskas**, V. Melissinaki, D. Kaškelytė, M. Farsari, and M. Malinauskas, Improvement of the fabrication accuracy of fiber tip microoptical components via mode field expansion, *J. Laser. Micro Nanoen.* **9**(1), 68–72 (2014).
- [A6] **A. Žukauskas**, G. Batavičiūtė, M. Ščiuka, T. Jukna, A. Melninkaitis, and M. Malinauskas, Characterization of photopolymers used in laser 3D micro/nanolithography by means of laser-induced damage threshold (LIDT), *Opt. Mat. Express* **4**(8), 1601-1-616 (2014).
- [A7] **A. Žukauskas**, G. Batavičiūtė, M. Ščiuka, Z. Balevičius, A. Melninkaitis, and M. Malinauskas, Effect of the photoinitiator presence and exposure conditions on laser-induced damage threshold of ORMOSIL (SZ2080), *Opt. Mater.* **39**, 224–231 (2015).
- [A8] **A. Žukauskas**, I. Matulaitienė, D. Paipulas, G. Niaura, M. Malinauskas, and R. Gadonas, Tuning the refractive index in 3D direct laser lithography: towards GRIN microoptics, *Laser Photon. Rev.* accepted DOI 10.1002/lpor.201500170 (2015).

#### *Conference proceedings*

- [A9] **A. Žukauskas**, K. Tikuišis, M. Ščiuka, A. Melninkaitis, R. Gadonas, C. Reinhardt, and M. Malinauskas, Single-step direct laser fabrication of complex shaped microoptical components, *Proc. SPIE* **8428**, 84280K (2012).
- [A10] **A. Žukauskas**, G. Batavičiūtė, M. Ščiuka, A. Melninkaitis, and M. Malinauskas, Laser-induced damage in photopolymers thin films with ultrashort pulses, *Proc. SPIE* **9130**, 913013 (2014).

#### *Other scientific papers*

- [A11] V. Osipov, V. Pavelyev, D. Kachalov, **A. Žukauskas** and B. Chichkov, Realization of binary diffractive optical elements by two-photon polymerization technique, *Opt. Express* **18**(25), 25808–25814 (2010).

- [A12] M. Malinauskas, D. Baltrikienė, A. Kraniauskas, P. Danilevičius, R. Jarašienė, R. Širmenis, **A. Žukauskas**, E. Balčiūnas, V. Purlys, R. Gadonas, V. Bukelskienė, V. Sirvydis, and A. Piskarskas, In vitro and in vivo biocompatibility study on laser 3D microstructurable polymers, *Appl. Phys. A.* **108**(3), 751–759 (2012).
- [A13] M. Malinauskas, G. Kiršanskė, S. Rekštytė, T. Jonavičius, E. Kaziulionytė, L. Jonušauskas, **A. Žukauskas**, R. Gadonas, and A. Piskarskas, Nanophotonics lithography: a versatile tool for manufacturing functional three-dimensional micro-/nano-objects, *Lith. J. Phys.* **52**(4), 312–326 (2012).
- [A14] M. Malinauskas, **A. Žukauskas**, K. Belazaras, K. Tikuišis, V. Purlys, R. Gadonas, and A. Piskarskas, Laser fabrication of various polymer micro-optical components, *Eur. Phys. J-Appl. Phys.* **58**, 20501 (2012).
- [A15] S. Rekštytė, **A. Žukauskas**, V. Purlys, Y. Gordienko, and M. Malinauskas, Direct laser writing of 3D polymer micro/nanostructures on metallic surfaces, *Appl. Surf. Sci.* **270**, 382–387 (2013).
- [A16] **A. Žukauskas**, M. Malinauskas, A. Kadys, G. Gervinskas, G. Seniūtinas, S. Kandasamy, and S. Juodkazis, Black silicon: substrate for laser 3D micro/nanopolymerization, *Opt. Express* **21**(6), 6901–6909 (2013).
- [A17] L. Jonušauskas, **A. Žukauskas**, P. Danilevičius, and M. Malinauskas, Fabrication, replication, and characterization of microlenses for optofluidic applications, *Proc. SPIE* **8613**, 861318 (2013).
- [A18] R. Buividas, V. Mizeikis, G. Kiršanskė, **A. Žukauskas**, M. Malinauskas, T. Murayama, Y. Hikima, J. Morikawa, and S. Juodkazis, Optical and thermal characterization on micro-optical elements made by femtosecond laser writing, *Proc. SPIE* **8923**, 89234X (2013).
- [A19] L. Rosa, G. Gervinskas, **A. Žukauskas**, M. Malinauskas, E. Brasselet, and S. Juodkazis, Optoplasmonics: hybridization in 3D, *Proc. SPIE* **8923**, 89231Q (2013).
- [A20] M. Malinauskas, **A. Žukauskas**, and K. Belazaras, Employment of fluorescence for autofocusing in direct laser writing micro-/nano-lithography, *Proc. SPIE* **9192**, 919212 (2014).
- [A21] T. Jonavičius, S. Rekštytė, **A. Žukauskas**, and M. Malinauskas, Laser nanolithography and chemical metalization for the manufacturing of 3D metallic interconnects, *Proc. SPIE* **8970**, 89700C (2014).
- [A22] S. Rekštytė, L. Jonušauskas, **A. Žukauskas**, G. Gervinskas, M. Malinauskas, and S. Juodkazis, Three-dimensional nanostructuring of polymer materials by controlled avalanche using femtosecond laser pulses, *Proc. SPIE* **8972**, 89721O (2014).
- [A23] M. Malinauskas, **A. Žukauskas**, S. Hasegawa, Y. Hayasaki, V. Mizeikis, R. Buividas and S. Juodkazis, Ultrafast laser processing of materials: from science to industry, *Light. Sci. Appl.* accepted (2015).

*Conference presentations*

- [C1] **A. Žukauskas**, K.K. Tikuišis, M. Malinauskas and R. Gadonas, Mikrooptinių elementų formavimas tiesioginio lazerinio rašymo metodu, LNFK, 2011 10 06, Vilnius, Lithuania (oral).

- [C2] **A. Žukauskas**, M. Malinauskas, C. Reinhardt, M. Ščiuka, A. Melninkaitis and R. Gadonas, Single step laser fabrication and integrated packaging of complex shaped microoptical components, SPIE Photonics Europe, 2012 04 16-20, Brussels, Belgium (oral).
- [C3] **A. Žukauskas**, M. Malinauskas, C. Reinhardt and R. Gadonas, Laser fabrication of complex shaped microoptical components and closely packed arrays of them, MSE, 2012 09 25–27, Darmstadt, Germany (keynote).
- [C4] **A. Žukauskas**, M. Malinauskas ir E. Brasselet, Aukštesnės eilės Beselio pluošto generacija vienalyčiu hibridiniu mikrooptiniu elementu, LNFK, 2013 06 06, Vilnius, Lithuania (poster).
- [C5] **A. Žukauskas**, V. Melissinaki, M. Malinauskas, M. Farsari and R. Gadonas, Fabrication and applications of fiber tip microoptical components, LAMP, 2013 07 25, Niigata, Japan (oral).
- [C6] **A. Žukauskas**, R. Gadonas and M. Malinauskas, Improvement of the laser fabrication technique for the fiber tip microoptical components, COLA, 2013 10 6–11, Ischia, Italy (poster).
- [C7] **A. Žukauskas**, G. Batavičiūtė, M. Ščiuka, A. Melninkaitis and M. Malinauskas, Optical resistance measurements of photopolymers used in direct laser writing lithography, LON, 2013 11 21, Vilnius, Lithuania (poster).
- [C8] **A. Žukauskas**, R. Gadonas and M. Malinauskas, Development of the direct laser writing technique for the fabrication of fiber tip microstructures, LON, 2013 11 21, Vilnius, Lithuania (poster).
- [C9] **A. Žukauskas**, G. Gervinskas, M. Malinauskas, A. Kadys, Z. Balevičius, R. Tomašiūnas and S. Juodkasis, Creation of high efficiency extractors of LED structures by means of laser lithography, SPIE Photonics West, 2014 02 05, San Francisco, USA (oral).
- [C10] **A. Žukauskas**, M. Malinauskas ir E. Brasselet, Optinių elementų integravimas ant šviesolaidžio ir jų naudojimas šviesai valdyti, Jaunųjų mokslininkų konferencija, 2014 02 11 Vilnius, Lithuania (oral).
- [C11] **A. Žukauskas**, G. Batavičiūtė, M. Ščiuka, A. Melninkaitis and M. Malinauskas, Laser-induced damage of photopolymer thin films induced by ns and fs laser pulses at various wavelengths, SPIE Photonics Europe, 2014 04 16, Brussels, Belgium (poster).
- [C12] **A. Žukauskas**, E. Brasselet and M. Malinauskas. Development of laser non-linear lithography technique for fiber end-face microoptical components, SPIE Photonics Europe, 2014 04 15, Brussels, Belgium (oral).
- [C13] **A. Žukauskas**, G. Batavičiūtė, M. Ščiuka, A. Melninkaitis and M. Malinauskas. Laser-induced damage in photopolymers thin films with nanosecond and femtosecond pulses, Nanotechnology: Research and Development, 2014 05 15, Vilnius, Lithuania (poster).
- [C14] **A. Žukauskas**, A. Kadys, R. Tomašiūnas and M. Malinauskas, Integration of the microoptical components for the light flow directionality control from light-emitting devices, LPM, 2014 06 20, Vilnius, Lithuania (oral).
- [C15] **A. Žukauskas**, A. Kadys, R. Tomašiūnas and M. Malinauskas, Manufacturing of the integrated microlenses via direct laser writing for the light flow control of UV LEDs, SPIE Optics+Photonics, 2014 08 20, San Diego, USA (oral).

- [C16] **A. Žukauskas**, I. Matulaitienė, D. Paipulas, G. Niaura, and M. Malinauskas, Relationship between the degree of conversion and refractive index in *fs* laser micropolymerized structures: towards GRIN microoptics, NOP, 2015 06 03, Imatra, Finland (poster).

## Contribution of the Authors

All experimental research described in this thesis was performed during 2011–2015 years in Vilnius University, Department of Quantum Electronics. Part of the experiments were carried out under *LaserLab-Europe* program in FORTH-IESL research institute and Vilnius University together with the colleagues from Greece (dr. M. Farsari and Ph.D. student V. Melissinaki) and France (dr. E. Brasselet). Direct laser writing, Raman spectroscopy and spectrophotometric characterization experiments were conducted by the author of the thesis. Laser-induced damage testing and ellipsometry measurements were performed in collaboration with co-workers. This thesis is an interdisciplinary work, spanning from laser technologies to polymer chemistry, and cannot be imagined without co-authors, whose contribution is listed below:

- Prof. **R. Gadonas** [A2, A3, A9] was a supervisor of this work and supported the doctoral research;
- Dr. **M. Malinauskas** [A1–A10] made it possible to carry out this research and is a main co-author of the majority of scientific articles. He helped to interpret and discuss the results as well as publish and present them at scientific conferences;
- Dr. **E. Brasselet** [A1, A4] initiated experiments described in chapters 4.3 and 4.4, performed theoretical calculations and conducted part of the experiments during the *LaserLab-Europe* visit in Vilnius. He is a main co-author of [A1, A4] publications;
- Dr. **A. Melninkaitis** [A6, A7, A9, A10] has introduced to laser-induced damage testing methodology and helped to publish the results;
- Dr. **M. Farsari** [A3, A5] provided the possibility to use hybrid prepolymer and consulted on questions related to this material's synthesis;
- Dr. **D. Paipulas** [A8] introduced and assisted during refractive index measurement experiments;
- Habil. Dr. **G. Niaura** [A8] helped to analyse Raman spectra and to determine their reliability;
- dr. **I. Matulaitienė** introduced to Raman spectroscopy method and was a technical consultant;
- Dr. **C. Reinhardt** [A2, A9] has performed finite-difference time-domain numerical analysis of the conical lenses and is a main co-author of [A2] publication;
- dr. **Z. Balevičius** [A3, A7] performed ellipsometry measurements;
- Ph.D. candidate **G. Batavičiūtė** [A6, A7, A10] analysed and interpreted the results of laser-induced damage testing;
- Ph.D. candidate **V. Melissinaki** [A5] was a main co-worker in integration of microoptical elements onto fiber tips during the practice in FORTH-IESL research center;

- **M. Ščiuka** [A6, A7, A9, A10] conducted laser-induced damage tests of polymers.

## **Structure of the Thesis**

The presented work is divided into five chapters:

- in Chapter 1, a brief overview of microoptical components' history, their classification and fabrication methods are provided. Additionally, the basics of the direct laser writing technique and its applications in the field of microoptics is given;
- in Chapter 2, the experimental setups used for the fabrication and characterization of the samples are described. Also, the synthesis process of the photosensitive material is explained and photopolymerization reactions are discussed;
- Chapter 3 is devoted for the determination of the polymers' laser-induced damage threshold;
- Chapter 4 begins from the description of the fabrication principles of the microoptical components. Next, the experimental results on the fabrication of conical lenses, spiral phase plates, bi-functional elements and their integration onto fiber tips are presented. In parallel, the generation of optical vortexes and higher order Gaussian-Bessel beams using fabricated elements is exploited;
- in Chapter 5, experimental realization of the gradient-index structure, resulting from a laser-induced local refractive index modification due to monomers' cross-linking, i.e. degree of conversion, is proposed and demonstrated.

At the end of this work, the results of this thesis are summarized and a list of conclusions is given.

---

## Review of the Literature

---

### 1.1 Microoptical elements: history, classification and fabrication methods

For the first time the term *microoptics* was mentioned by Dr. T. Uchida and Dr. I. Kitano in the late 1960's [4], but some scientists argue that this term appeared in literature in 1984 [5,6]. Nevertheless, the roots of microoptics reach much further back in the history. It was in 17th century when the pioneers of the microscopy and microbiology, *Antonie van Leeuwenhock* and *Robert Hooke*, have melted small filaments of glass and used them as lenses for their „under construction” microscopes [7]. At that moment, the progress of the microoptics has started. In 18th century *David Rittenhouse* has constructed the first diffraction grating out of human hairs while *Joseph von Fraunhofer*, in 19th century, has derived the law of diffraction and measured the wavelength of the light. The latest breakthrough in microoptics has started in the 8th decade of the 20th century when manufacturing techniques from semiconductor industry were adapted for the fabrication of diffraction gratings. It was followed by the demonstration of the refractive microoptical elements' fabrication one decade later [8–10] and continuous surface profile components at the end of the 20th century [11]. This motivated the research and continuous development in the field of microoptics which is moving towards practical applications these days [12,13].

Examples of the microoptical components can be found in nature all around us. Compound eyes of the insects and crustaceans are made of many repeatable units (ommatidia) and each of them is composed of a microlens. In some cases wings of the butterflies and birds' plumes reminds the diffraction gratings. Meanwhile, dew drops on plant leaves acquire hemispherical surface shape due to condensation and are similar to the microlenses fabricated using self-formation technologies (e.g. resist reflow).

Generally, microoptical components can be classified into two main groups according to the light confinement within the element: (1) waveguide optics (the propagation of the light is restricted by a refractive index distribution), and (2) free-space optics (the light is not confined). Due to the large diversity of the MOCs, we are going to focus on the latter elements. Moreover, four types of the free-space optical elements can be distinguished in respect to their feature size ( $\Gamma$ ) and light wavelength ( $\lambda$ ): (1) refractive continuous surface profile MOCs ( $\Gamma \gg \lambda$ ), (2) refractive

periodic structures of continuous profile ( $\Gamma \geq \lambda$ ), (3) periodic sub-wavelength structures ( $\Gamma < \lambda$ ), and (4) combination of above mentioned elements (e.g.  $\Gamma \gg \lambda$  and  $\Gamma \geq \lambda$ ). According to this nomenclature, let us narrow the subject of this research up to the first and the fourth groups.

For a long time classical cutting, grinding and polishing techniques were used for the manufacturing of the optical components. However, these methods reach their limits and capabilities when the size of the optical elements decreases below 1 mm. In this case, the development of novel methods and adaptation of the mask-based lithography techniques from the field of integrated circuits allowed to enter a new stage for the microoptical elements. Currently, a huge variety of the fabrication methods exists and it is not possible to discuss all of them in details. Therefore, a classification and brief overview of the fabrication methods will be given in this section meanwhile the peculiarities of each technique can be found in the following books [4–6, 14]. Commonly, MOCs’ manufacturing techniques can be grouped into three categories in respect to the principles of the fabrication: (1) lithographic, (2) self-formation, and (3) subtractive techniques (see Fig. 1.1). In the first case, a photosensitive material on the substrate is exposed to the light so that its pattern, encoded as an amplitude distribution, is embedded into the material due to photopolymerization. The illumination of the sample can be realized either through the mask (binary, multi-level [15] or grey tone [16]) or scanning the sample point-by-point with a focused beam of electrons [17] or light [18]. The former methods are distinguished

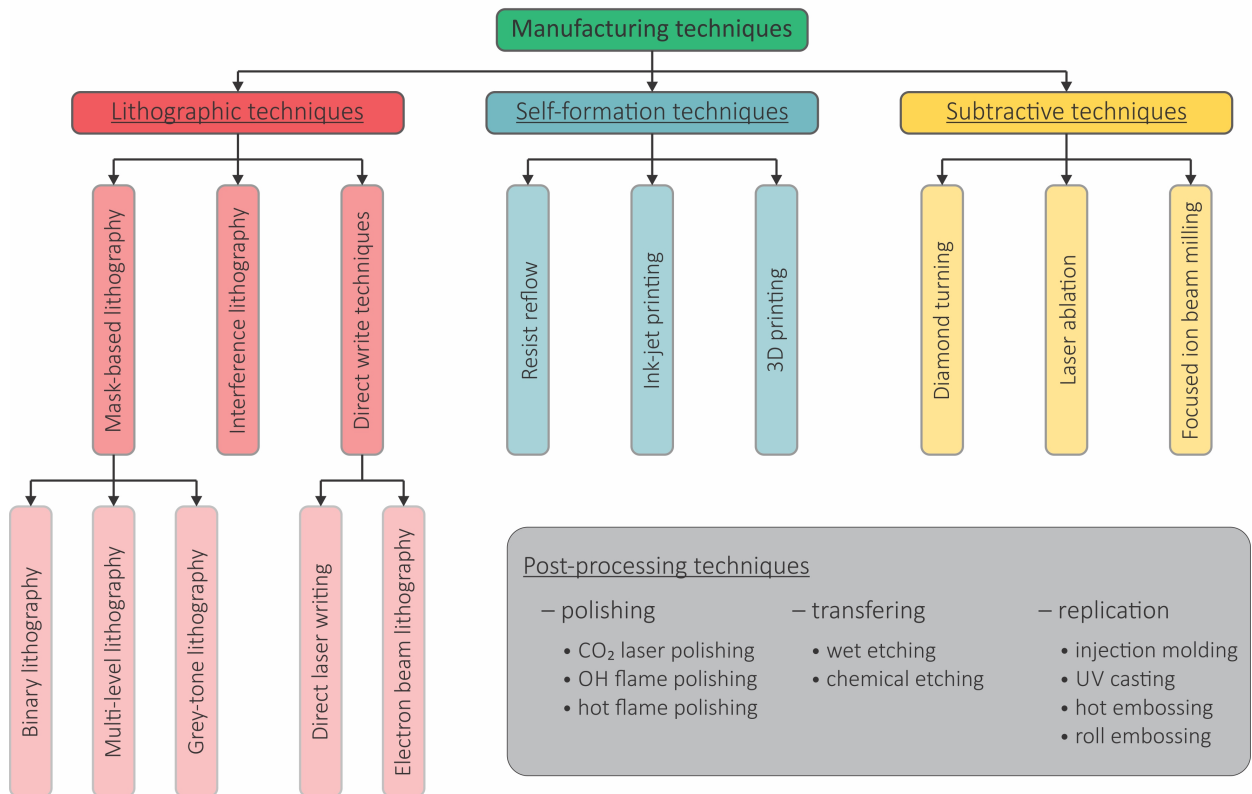


**Fig. 1.1:** Classification of the microoptical elements’ manufacturing and post-processing techniques.

by the high throughput, short exposure time and low fabrication costs whereas the latter – by high flexibility and arbitrary design of the MOCs. Also MOCs’ fabrication over a large area in a short time can be carried out via interference lithography technique when the intensity pattern of the several laser beams is transferred into exposed light sensitive material, although in most cases only a periodic structures can be produced [19]. In the second case, the fabrication method is based on the surface tension of the polymer’s cylinders [11], droplets [20] or filaments [21] by heating them above their glass transition temperature. During melting, surface tension leads to the formation of spherical and/or cylindrical lenses as material tries to acquire a shape which satisfies the condition of the lowest energy, i. e. to gain minimal surface area. MOCs, fabricated using self-formation techniques, are benefiting from the high sphericity, very smooth surface, low price and large-scale production. The last fabrication method is based on the material’s removal during the interaction with a diamond tool [22], focused laser [23] or ion beam [24]. The biggest advantage of this technique lies in the ability to process various materials (plastics, glasses, metals and semiconductors).

Even though a large variety of techniques for the fabrication of the MOCs exists, in some cases the quality of the produced elements is not satisfactory and the components should be post-processed. For example, the surface roughness of the MOCs can be increased by polishing with a CO<sub>2</sub> laser, OH gas flame or heating. Meantime, the elements, fabricated out of polymers, can be transferred into glass by wet and/or dry etching. Moreover, some of the aforementioned fabrication methods suffer from low throughput which is undesirable in terms of mass production, but it can be overcome by employing a variety of replication techniques.

## 1.2 Direct laser writing technique: principles and applications

The first experimental demonstration of the direct laser writing technique was published in 1997 [2]. Over the last 20 years this technique proved to be as a versatile tool for the rapid fabrication of custom-shaped 3D microstructures and has made a great stride in transition from the scientific laboratories to the industry. Four stages of the DLW process can be distinguished: (1) preparation of the material, (2) fabrication process, (3) development stage, and (4) characterization of the fab-

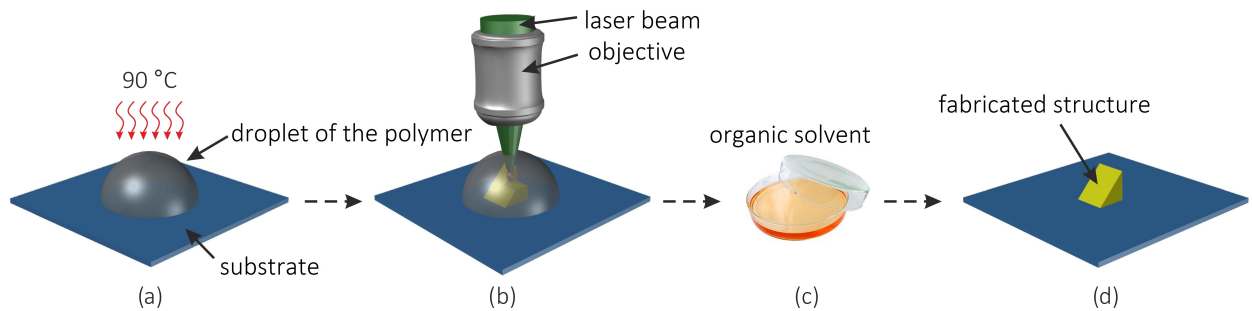


**Fig. 1.2:** Schematic illustration of the DLW fabrication process: (a) preparation of the material, (b) fabrication process, (c) development stage, and (d) characterization of the fabricated microstructure.



ricated microstructure (see Fig. 1.2). The DLW technique in the form of radical multi-photon polymerization is based on the simultaneous absorption of two or more photons of the same frequency in photosensitive molecules which subsequently undergo a radicalization process. The photogenerated radicals induce a cross-linking of prepolymeric materials. Due to the nonlinear interaction between the light and the prepolymer spin-coated or drop-casted on the glass substrate (Fig. 1.2 (a)) the photochemical reaction is highly confined inside the volume of the tightly focused laser beam. 3D structures are fabricated point-to-point: voxels (*volumetric pixels*) are formed in the bulk of the prepolymer by changing the position of the focus point according to the computer aided design (CAD) or the programmed code (Fig. 1.2 (b)). The light exposed negative prepolymer becomes insoluble in the organic solvent used as developer (Fig. 1.2 (c)), while the unexposed prepolymer is dissolved and washed out, leaving free-standing 3D microstructures with various geometries on arbitrary substrate (Fig. 1.2 (d)). The principles of the DLW process are described in more details in the following review papers [25–33].

Nine years after the invention of DLW technique, it has found numerous applications in the field of microoptics. At the early stage, the fabrication of classical minimized optical elements (lenses, prisms) was demonstrated [34,35], and then the manufacturing of more complex shaped elements has started [36–39]. Much efforts have been devoted for the process optimization and to overcome low fabrication throughput. For instance, implementation of various scanning strategies [3, 40] and outer shell fabrication [41–43], integration of the spatial light modulators for parallel multi-beam processing [44, 45], synthesis of novel materials [46] and other technical solutions [47, 48] allowed to speed-up the process up to 1000× and to fabricate a centimeter-sized objects [49]. In 2010, the first experimental demonstration of the MOCs’ integration on the fibers has appeared. Up to now, it has expanded considerably and fiber tip structures are used as Fabry-Pero, SERS (surface-enhanced Raman scattering) and acousto-optical sensors [50–52]. Moreover, microoptical elements fabricated by DLW technique are used in microfluidics [53], anti-reflective coatings [54], colour filters [55], LEDs (light emitting diodes) [56] and VCSELs (vertical-cavity surface emitting laser) [57]. This demonstrates a wide range of MOCs applications and development of the DLW fabrication method, which is still continuing.

---

## Experimental Methods

---

### *Materials used in fabrication*

Hybrid organic-inorganic prepolymer SZ2080 was used in this work. It was chosen because of the transparency in VIS and NIR ranges, mechanically and chemically stability, nearly glass matching refractive index, surface roughness down to sub-10 nm and possibility for doping with quantum dots, nanoparticles and fluorescent dyes [58]. It is synthesized via sol-gel process of the methacryloxypropyl trimethoxysilane (MAPTMS), methacrylic acid (MAA) and zirconium *n*-propoxide (ZPO). MAPTMS and MAA serve as organic polymerizable units while ZPO together with the alkoxysilane groups of MAPTMS act as inorganic moieties. During hydrolysis and polycondensation reactions the  $\text{-O-Si-O-Zr-O-}$  inorganic network with the attached methacrylic groups is formed. The inorganic network with the single bonds between the atoms serves as a back-bone of the molecule while methacrylic groups are responsible for the polymerization reaction. In addition, SZ2080 is photosensitized with the Irgacure 369 photoinitiator (2-benzyl-2-(dimethylamino)-1-[4-(4-morpholinyl) phenyl]-1-butanone). The synthesis process of the SZ2080 is described elsewhere in more details [58]. Upon absorption of the light, the C–C bond of the photoinitiator is broken and two highly reactive radicals are formed. Subsequently, C=C double bond in the methacrylic group is opened and converted to a C–C single bond. That initiates chain reaction which lasts until two free-radicals react with each other.

Samples were prepared by drop-casting the prepolymer on a cover glass and subsequently drying on a hotplate at three stages: (1) 20 min at 40 °C, (2) 20 min at 70 °C and 3) 20 min at 90 °C. After fabrication, the samples were developed in 4-methyl-2-pentanone for 1 hour. In order to minimize the effect of shrinkage due to capillary forces, the samples described in Chapter 5 were additionally developed in a critical point dryer. Afterwards, the samples were inspected with a differential interference contrast microscope. Scanning electron microscope (SEM) and optical profilometer were used for the quantitative analysis: determination of MOCs dimensions (height, radius), surface roughness, waviness and profile.

### *Fabrication method*

DLW setup equipped with Yb:KGW laser emitting 300 fs duration pulses at repetition rate of 200 kHz and second harmonic at 515 nm was used for the fabrication of

microoptical components. An immersion objective lens with a numerical aperture of 1.4 and a magnification  $100\times$  was used for tight focusing of the light into the volume of the prepolymer to induce the photochemical reaction. The laser spot was traced through the prepolymer by changing the position of the sample using linear air bearing motor stages. The laser intensity was attenuated by using a  $\lambda/2$  waveplate combined with a polarizer while the exposure time was adjusted using an acousto-optic modulator. A red light LED source, an objective lens and an additional lens together with a CCD camera were used for real time monitoring of the fabrication process. For the fabrication of MOCs on the fiber tip, home-made fiber holder was used and installed into setup. More details on this issue will be provided in Chapter 4.

### *Optical characterization of the samples*

Optical performance of the fabricated devices was tested regarding the propagation features of the generated light field. Three different experimental setups were used for the evaluation of amplitude, phase and refractive index properties. All of them include a 632.8 nm spatially filtered and  $7.5\times$  expanded He-Ne laser as a light source. In addition, the first configuration consists of microscope elements fixed on a micrometer stepper motor stage and a CCD camera. A Gaussian laser beam is focused at normal incidence onto the sample in the focal plane, where the fabricated MOC is placed. The intensity profiles at a distance  $z$  from the midplane of the structure were recorder by means of an objective lens and a CCD camera. Using the cover glass as a reference plane, the emergence and propagation of a Gaussian and/or Bessel beam can be observed.

For the evaluation of the phase properties of the generated light fields, the experimental setup was upgraded with a Mach-Zehnder interferometer consisting of two additional beam splitters and mirrors. In this case, the probe beam passes through the sample and interference with a reference beam passing through free-space occurs. In respect of focused laser beam size  $\omega_0$  and radius of the microoptical element  $r$ , only the  $\omega_0/R \leq 1/2$  case was considered in order to avoid diffraction by the outer part of the MOC which causes additional interference effects.

The refractive index was measured with the Michelson's interferometer instead of Mach-Zehnder's. A laser beam passes through the fabricated element and is magnified with an objective lens, split into two beams and reflected backwards resulting in a superposition beam. The arising intensity pattern is subsequently imaged onto a CCD camera. By adjusting one of the mirrors an interference pattern with equally spaced straight and parallel lines is obtained. The gradation of the fringes apparent in the pattern is the result of the interference between the laser beam propagating through the microstructure and reference beam (air) and can be used for the precise determination of refractive index.

### *Laser-induced damage threshold measurements*

A nanosecond Q-switched Nd:YAG and a femtosecond mode-locked Yb:KGW laser systems were used for the LIDT measurements according to ISO 21254-2:2011 standard [59] in 1-on-1 and S-on-1 ( $S \leq 1000$ ) regimes by using automated test station [60, 61]. The *ns* laser emitted  $\lambda = 1064$  nm wavelength pulses which were

frequency doubled to  $\lambda = 532$  nm. The pulse durations were 11 ns and 6.2 ns at 50 Hz repetition rate, respectively. The laser beam was focused to  $250 \pm 10 \mu\text{m}^2$  and  $133 \pm 4 \mu\text{m}^2$  spots at  $1/e^2$  intensity level in the sample plane, respectively to the first and second harmonics. In the case of the *fs* laser system, it provided 343 fs duration pulses at 1030 nm and 515 nm wavelengths while the repetition rate was set to 50 kHz. The laser beam was focused to  $65 \pm 0.2 \mu\text{m}^2$  beam spot at 1030 nm and  $46.5 \pm 0.2 \mu\text{m}^2$  at 515 nm. The measurement procedure was performed in an automated manner by a computer controlled sample positioning, laser fluence attenuation and damage detection system. *On-line* damage detection *in situ* was based on the change in optical scattering of irradiated site. Additionally, *off-line* damage inspection was performed registering laser-induced changes with differential interference contrast microscope at  $40\times$  magnification. Morphological surface examination of thin films was performed with scanning electron microscope. 20 nm gold layer was sputtered on top before the inspection with SEM.

### *Characterization of spectrophotometric and chemical properties*

The spectral distribution of the thin films' transmittance and reflectance was measured at close to normal incidence in the wavelength range of 190–1100 nm using double beam spectrometer. The obtained data were used for the determination of the absorption coefficient and the energy difference between the ground and the lowest excited states ( $\Delta E$ ) according to Tauc model [62].

Complex refractive index of the polymer SZ2080 was measured using standard ellipsometry technique. Spectral ellipsometer with two rotating compensators was used for the investigation into the optical response of polymers' coatings. Ellipsometric measurements have been carried out in the wavelength range from 240 nm to 1000 nm and angle of incidence  $\text{AOI} = 75^\circ$ . The obtained data were analysed by a multi-layer model. It represented the following layer sequence structure: Si substrate/polymer film/air. Optical constants of SZ2080 layers were characterized by Cody-Lorentz function in the regression analysis. The contribution of surface roughness was taken into account in the calculations of ellipsometric parameters  $\Psi(\lambda)$  and  $\Delta(\lambda)$ .

Raman spectra of the samples were measured with a confocal Raman microspectrometer in the  $830\text{--}1920 \text{ cm}^{-1}$  range. A cw He-Ne laser operating at 633 nm wavelength was used for the excitation via objective with the numerical aperture of 0.75. A laser beam of 5 mW average power was focused to a spot of  $1.3 \mu\text{m}$  in radius. Before the spectra acquisition, each sample was continuously irradiated for 15–30 min in order to reduce the fluorescence background. After the photo-bleaching, Raman spectra remained stable during acquisition, indicating the absence of additional polymerization or degradation effects in the sample. The irradiation time for each measurement was set to 10 s and the number of accumulations to 10, yielding a total accumulation time of 100 s. A 5th order polynomial function was used for the baseline subtraction. Each peak was fitted using a Lorentzian function, from which the peak data (height, integrated area, full width at half maximum, and position) were deduced.

---

## Investigation of the Polymers' Optical Resistance

---

*Material related to this chapter was published in [A6, A7, A10] and presented at [C7, C11, C13] conferences.*

Direct laser writing based lithography is an already established technique widely used for the rapid and flexible manufacturing of diverse three-dimensional (3D) micro/nano-objects [2,32]. Up to know, numerous state-of-the-art applications of the microoptical components have been demonstrated [3,37,63–65]. Much efforts have been devoted for the improvement of the microoptical components' optical quality in terms of surface roughness, transmittance, refractive index, shrinkage, etc [58,66,67]. For this purpose, various technical and scientific problems have been investigated and solved [40,41]. Besides, a vast number of light sensitive materials were employed for the manufacturing of the microoptical elements in order to meet the requirements of particular applications. However, integration of the MOCs fabricated via DLW technique into 3D optical circuits and their practical implementation is still limited. One issue which has not been considered and could be a limiting factor is a laser-induced damage threshold (LIDT).

The scope of this chapter is to characterize optical resistance of the polymers widely used for the manufacturing of 3D microstructures via DLW technique in long and ultra-short pulse duration regimes. In the first part of this chapter a special attention is given to a pure and photosensitized SZ2080 material used within this work and in the second part – the obtained results are compared with other types of polymers for which LIDT was determined as well.

### 3.1 Spectrophotometric characterization results

The transmission spectra of the pure and PI doped SZ2080 are shown in Fig. 3.1 (a). It is evident that both materials are transparent in the VIS and NIR spectral ranges, but in UV transmittance differs. Substantive difference between these materials lies in the fact that one of them is doped with PI in order to increase the sensitivity to the light before the fabrication. The PI's molecules are consumed during the initiation process of polymerization, even though some unreacted molecules remain in the polymer matrix after the fabrication. The influence to the absorption of these unreacted molecules is reflected by the differential spectrum. This absorption band

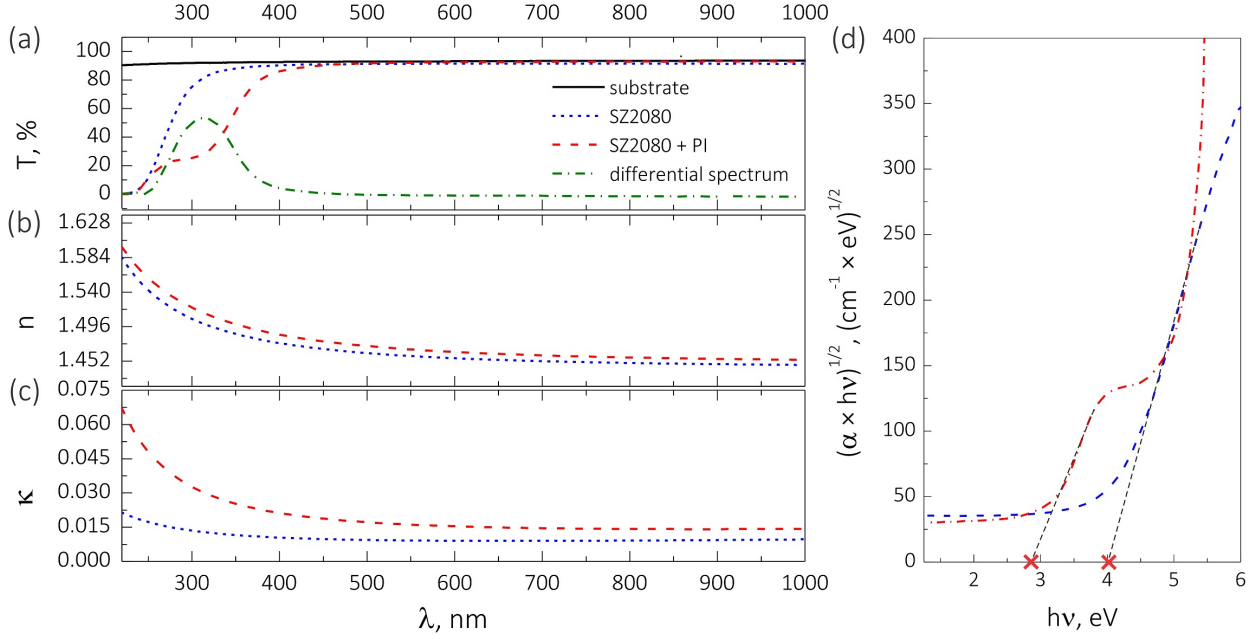


**Fig. 3.1:** The transmittance spectrum of the photosensitized and non-photosensitized SZ2080 thin films (a), real (b) and imaginary (c) parts of the refractive index dispersion curves. (d) Determination of the  $\Delta E$  according to Tauc method [62].

is attributed to the  $\pi - \pi^*$  transition in the aromatic groups of PI. In Fig. 3.1 (b) the real parts of the complex refractive index of the pure SZ2080 and SZ2080 + PI are shown. Both materials are distinguished by the normal dispersion. The variation of the refractive index over a range from 1.447 to 1.554 for pure SZ2080 and from 1.454 to 1.570 for SZ2080 + PI is apparent in the 240–1000 spectral range. The energy difference between the ground and the lowest excited states is estimated from a linear extrapolation of  $(\alpha \times hv)^{1/2}$  versus photon energy ( $hv$ ) to a zero near the absorption edge. The analysis of the Tauc plots reveals that  $\Delta E$  of the pure SZ2080 and SZ2080 + PI is 4.03 eV and 2.72 eV, respectively (Fig. 3.1 (d)). Thus, the presence of the PI and its concentration in the host matrix of the hybrid polymer allows to tailor the refractive index as well as the energy difference between the ground and the lowest excited states.

### 3.2 Nano- and femtosecond pulses induced damage of the SZ2080

LIDT values of the pure and photosensitized SZ2080 for the 1-on-1 and S-on-1 cases at the first and second harmonics in the *ns* and *fs* pulse duration regimes are summarized in Table 3.1. The obtained values of the LIDT are in the range of tens J/cm<sup>2</sup> in the *ns* pulse mode and an order of magnitude lower in the *fs* pulse mode. Also, it can be seen that damage threshold of the pure SZ2080 is higher or comparable within error limits than that of the SZ2080 + PI in all cases. Moreover, the attained results at the second harmonics and S-on-1 regime indicate that avoidance of the photosensitization leads to higher resistance to the laser irradiation. Obviously, higher extinction coefficient (Fig. 3.1 (c)) and lower  $\Delta E$  energy result in increase of the absorption which yields a more efficient laser energy transfer via free electron

**Table 3.1:** Experimentally measured laser-induced damage threshold values (J/cm<sup>2</sup>) at single and multi-shot regimes.

Polymer	Regime	<i>ns</i> pulse test		<i>fs</i> pulse test	
		532 nm	1064 nm	515 nm	1030 nm
SZ2080	1-on-1	16.69 ± 1.72	21.00 ± 2.88	0.68 ± 0.12	1.39 ± 0.16
	S-on-1	13.67 ± 1.31	14.73 ± 2.10	0.13 ± 0.10	0.57 ± 0.08
SZ2080 + PI	1-on-1	13.75 ± 1.01	22.98 ± 1.72	0.55 ± 0.08	1.46 ± 0.12
	S-on-1	1.44 ± 0.28	10.63 ± 1.07	0.06 ± 0.04	0.49 ± 0.05

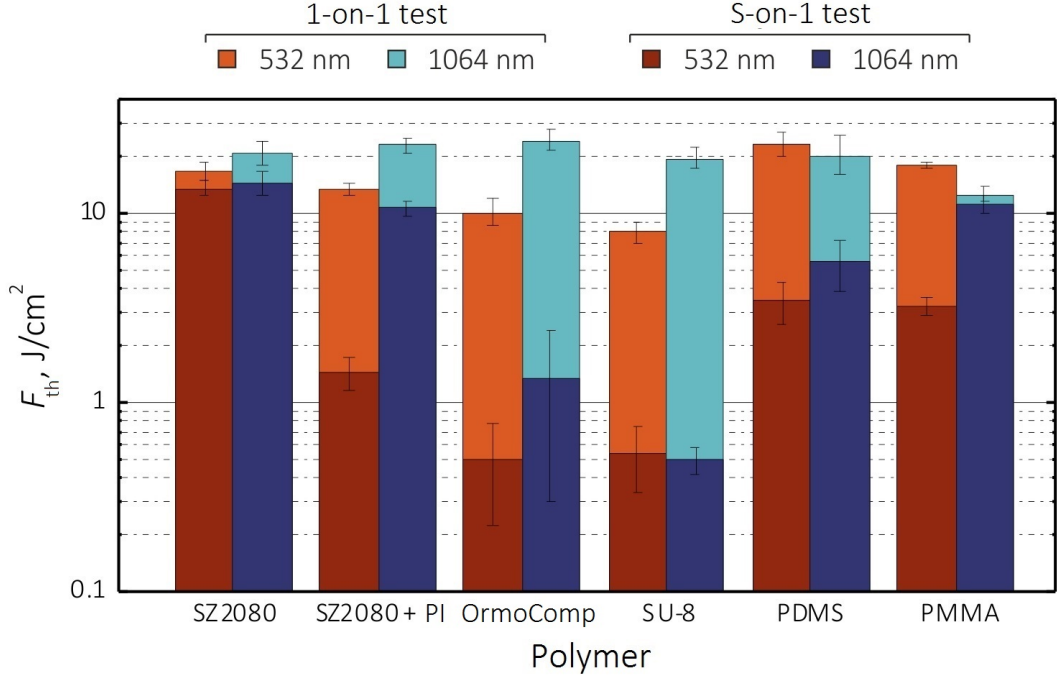
generation to the lattice which in turn causes optical breakdown and reduction of the damage threshold of the SZ2080 + PI. S-on-1 regime tests revealed that LIDT of all samples is decreasing with the increase of the pulse number. This phenomena is attributed to the thermal accumulation and chemical bond breaking effects which can be quantitatively evaluated according to the model proposed by Jee [68]. It relates LIDT fluence  $F_{th}(N)$  to the 1-on-1 threshold fluence  $F_{th}(1)$  by the following expression:

$$F_{th}(N) = F_{th}(1) \times S^{\xi-1}; \quad (3.1)$$

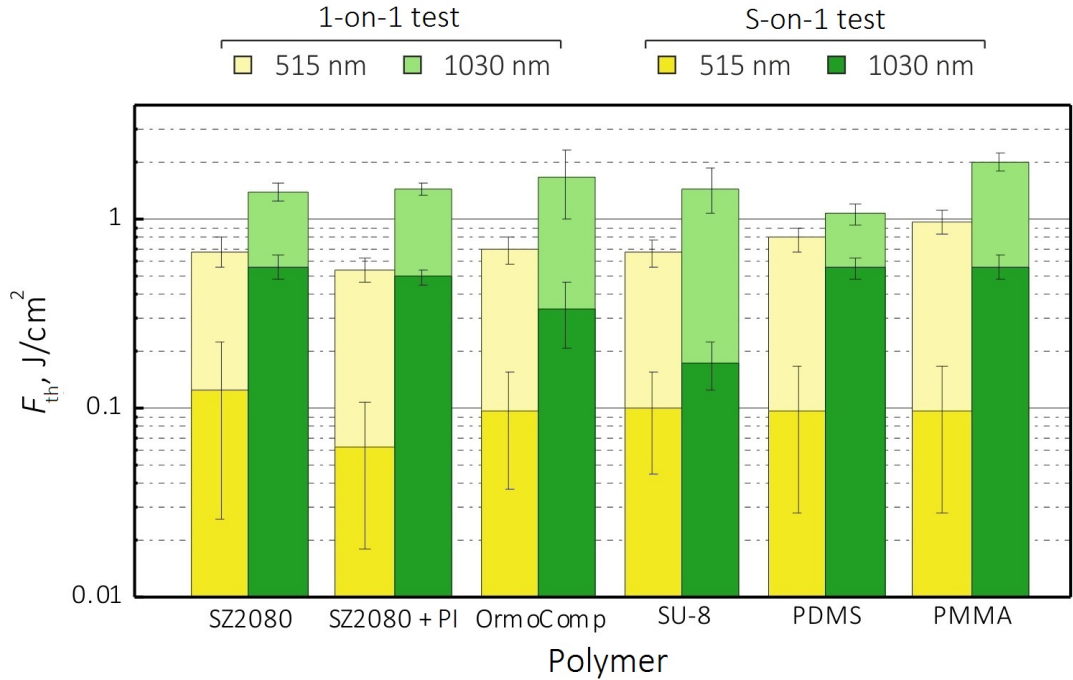
here  $\xi$  is an incubation parameter and  $N$  – number of pulses.  $\xi = 1$  means that no incubation effect can be observed. By applying the present model we have obtained that  $\xi$  ranges from 0.88 to 0.97 at *ns* pulse mode and from 0.68 to 0.87 at *fs* pulse mode. It indicates that the effect of incubation occurs in all cases. Moreover, analysis of the damage morphology revealed that delamination of thin films in all cases can be observed at long pulse regime. Meanwhile, at ultra-short pulse regime, the damage morphology is different – only the surface of the coating is affected and its microexplosion or ablation can be identified.

### 3.3 Laser-induced damage threshold of other polymers

Experimental values of the LIDT for the various polymers (SZ2080 + PI, SZ2080, OrmoComp, SU-8, PDMS and PMMA), exposed to nanosecond and femtosecond pulse duration radiation, are shown in Fig. 3.2 (a) and (b), respectively. For the direct comparison of how the wavelength and the number of pulses influence laser-induced damage threshold, results are plotted on the same graph for the fundamental (1064 nm and 1030 nm) and the second (532 nm and 515 nm) harmonics at single (1-on-1) and multi-shot (S-on-1) regimes. Obtained LIDT values of polymers range from  $\approx 8$  J/cm<sup>2</sup> to  $\approx 25$  J/cm<sup>2</sup> at single-shot regime and from  $\approx 0.3$  J/cm<sup>2</sup> to  $\approx 15$  J/cm<sup>2</sup> at multi-shot regime for nanosecond pulse duration case. Measurements of the damage threshold fluence at femtosecond pulse duration laser radiation and multi-shot regime revealed that LIDT decreases by one or two orders of magnitude in comparison to the results at *ns* pulses:  $\approx 0.1$  J/cm<sup>2</sup> and  $\approx 0.2$ – $0.6$  J/cm<sup>2</sup> at 515 nm and 1030 nm wavelengths, respectively.



(a) *ns* pulse regime (experimental conditions: Nd:YAG laser system,  $f = 50$  Hz,  $\tau = 11$  ns and 6.2 ns,  $\omega_0 = 250.2 \pm 10.0$   $\mu m$  and  $133.5 \pm 4.6$   $\mu m$  for the first (1064 nm) and second (532 nm) harmonics, AOI =  $0^\circ$ ).



(b) *fs* pulse regime (experimental conditions: Yb:KGW laser system,  $f = 50$  kHz,  $\tau = 343$  fs,  $\omega_0 = 65.0 \pm 0.2$   $\mu m$  and  $46.5 \pm 0.2$   $\mu m$  for the first (1030 nm) and second (515 nm) harmonics, AOI =  $0^\circ$ ).

**Fig. 3.2:** Column diagrams showing LIDT of polymers thin films at *ns* (a) and *fs* (b) pulse regimes for the first and second harmonics and 1-on-1 and S-on-1 tests.



*Nanosecond pulse induced damage mechanisms*

Generally, polymers can be classified into two groups: saturated and conjugated compounds. The difference between these two groups lies in the chemical bond type between carbon atoms along the polymer backbone, i.e. whether it is single (saturated) or alternating single-double (conjugated). In our case, PMMA and PDMS can be assigned to the saturated polymer class whereas SU-8 belongs to conjugated polymer class due to electron delocalization in benzene rings. Attribution of the SZ2080, SZ2080 + PI and OrmoComp for any single class is more complicated. It is likely that pure SZ2080 belongs to the saturated polymer class [58]. However, doping of the polymers with the PIs, which are typically conjugated compounds, changes their optical properties significantly. Therefore, we can assume that SZ2080 + PI and OrmoComp is a mixture of the saturated and conjugated compounds.

Laser-induced damage measurements at single-shot regime and 532 nm indicate that the highest LIDT is characteristic for saturated polymers (PDMS, PMMA and SZ2080) and the lowest – for conjugated polymers (SZ2080 + PI, OrmoComp and SU-8). The number of alternating single-double bonds is the highest for the SU-8 in comparison to OrmoComp and SZ2080 + PI and it explains the lowest damage threshold of SU-8. Such LIDT correlation with the polymers' type can be explained by the fact that electron binding energy is higher for the saturated compounds than for the conjugated. It means that lower laser fluence is necessary in order to break chemical bond of the conjugated polymers in comparison to saturated.

*Femtosecond pulse induced damage mechanisms*

In the last decade it was shown that simultaneous absorption of  $n$  photons with the sum energy equal to  $\Delta E$  or higher is one of the leading mechanisms of optical breakdown for dielectric layers at ultra-short pulses regime [69, 70]. This idea is supported by the evidence of the empirical data of LIDT cascade dependence on the  $\Delta E$  energy. Abrupt increase of the damage threshold was observed at the point where  $n + 1$  instead of  $n$  photons were required for the absorption. In order to verify this hypothesis for the polymers, we have plotted LIDT as a function of  $\Delta E$ . We have noticed an increase of the damage threshold value from  $\approx 0.65$  J/cm<sup>2</sup> to  $\approx 0.9$  J/cm<sup>2</sup> between  $n = 2$  and  $n = 3$  cases at single-shot regime. This reveals that multiphoton absorption is probably a dominant process for the optical breakdown as a higher intensity is necessary for the absorption of three photons instead of two. Meanwhile optical damage at multi-shot regime is influenced by either thermal accumulation or chemical bond breaking effects as LIDT values decrease up to  $\approx 0.1$  J/cm<sup>2</sup> and no cascade behavior can be observed [71]. In the case of measurements at 1030 nm wavelength we did not notice any correlation between LIDT and  $\Delta E$  of the polymers. The probability of  $n$  photon absorption scales as  $P \propto I^n \sigma_n \tau$ , where  $I$  is intensity of the light,  $\sigma_n$  – absorption cross-section of  $n$  photons and  $\tau$  – pulse duration [72]. It becomes negligible small at longer wavelengths as higher number of photons is necessary for the transition. Together with the absence of LIDT's dependence on  $\Delta E$ , it implies that multiphoton absorption is not a predominant mechanism of optical damage at 1030 nm wavelength and it is likely that other phenomenon have bigger influence.

---

## Singular Optical Components

---

*Material related to this chapter was published in [A1–A5 ir A9] and presented at [C1 – C6, C8, C10 ir C12] conferences.*

In this chapter, the experimental results on fabrication of singular microoptical components will be discussed. In each section, we present the results on the fabrication of a different microoptical element and discuss the features of the light beam propagation through them.

### 4.1 Fabrication of the microoptical components

Beam shaping of light using micron scale optical devices remains a contemporary challenge for the development of integrated optics, especially when the generation of optical singularities is considered. In fact, to imprint singular features onto a light beam from an element with typical spatial dimension, e.g. the radius  $R$ , basically requires an optical component endowed with an appropriate topological structuring having a spatial resolution  $\delta l \ll R$ . Consequently, the smaller  $R$ , the more stringent is the constraint on  $\delta l$ . In practice, the first thing that must be determined is the dependence of the size of the photopolymerized volumetric pixel (i.e. feature size  $\delta l$ ) on the DLW processing parameters: average laser beam power and scanning speed. For this purpose, „resolution bridge” method was employed [73]. The obtained results allow to define the voxel overlap which is a determining factor of the MOCs surface roughness and geometrical shape accuracy:  $\delta = [(d-dz)/d] \times [(l-dx)/l] \times 100$ , here  $\delta$  is the degree of the voxel overlap,  $d$  and  $l$  are the transverse and longitudinal dimensions of the voxel, respectively, and  $dz$  and  $dx$  are the transverse and lateral scanning steps, respectively. In our case, when the scanning step becomes higher than  $\delta \approx 90\%$ , the surface roughness is below 10 nm and the  $\lambda/10$  criteria for the MOCs surface is met at the VIS spectral range. The degree of the voxel overlap is only one of the many parameters allowing to fabricate smooth surface MOCs. The others are various scanning modes and fabrication algorithms (concentric ring or spiral scanning), shape precompensation due to shrinkage leading to the shape deformations and distortions, the choice of the appropriate materials and development conditions. To summarize, at first glance DLW technological processes are trivial, but they are the basis for the fabrication of high quality microoptical elements.

## 4.2 Conical microlenses

An axicon is an optical element with a surface profile defined by a  $360^\circ$  rotated prism. Compared to conventional optical elements, the transverse intensity distribution of light passed through the conical lens is described by a Bessel function. It allows achieving theoretically nondiffracting beams in the long focal range distances with a linear growth of the on-axis intensity. To demonstrate the flexibility and feasibility of the DLW technique, three types of the conical lenses with various cone angles ( $150^\circ$ ,  $160^\circ$  and  $170^\circ$ ) and  $15\ \mu\text{m}$  radius were fabricated. SEM image of the  $150^\circ$  cone angle axicon is shown in Fig. 4.1 (a). As one can observe, a small tip with a radius of  $500\ \text{nm}$  is seen on the top which is caused by an overexposure. The tip determines the curvature radius of the conical lens' top and can cause the on-axis intensity fluctuations of the Bessel beam [74]. In our case, the approximation of the conical lens top with a circle has shown that the curvature radius of the tip is equal to  $2.5\ \mu\text{m}$  (Fig. 4.1 (b)). Nevertheless, the analysis of the various cone angle axicons' geometrical properties (cone angle, radius and height) performed with an optical profilometer revealed that fabricated axicons are in close coincidence with the designed structure. Optical performance of the  $150^\circ$ ,  $160^\circ$  and  $170^\circ$  cone angle axicons was measured with a setup described in Chapter 2. The obtained results show the formation of the Bessel beam profile with  $100 \pm 5\ \mu\text{m}$ ,  $150 \pm 5\ \mu\text{m}$  and  $210 \pm 5\ \mu\text{m}$  maximum propagation distance, defined as  $z_{max} \approx \omega/(n-1)\psi$ , to  $150^\circ$ ,  $160^\circ$  and  $170^\circ$  cone angle axicons, respectively. Moreover, in agreement with theoretical calculations of the Bessel beam with  $r_0 = 2.405/k_\perp$  (here  $k_\perp = k(n-1)\psi$ ), we observe a central spot size dependence on the cone angle. As the cone angle decreases, the diameter of the Bessel beam central spot increases: calculated values for  $150^\circ$ ,  $160^\circ$  and  $170^\circ$  cone angles –  $1.84\ \mu\text{m}$ ,  $2.76\ \mu\text{m}$  and  $5.51\ \mu\text{m}$ ; measured values –  $2.12\ \mu\text{m}$ ,  $2.99\ \mu\text{m}$  and  $5.59\ \mu\text{m}$  (Fig. 4.1 (c) – (e)). Lastly, we have demonstrated the fabrication of a closely packed hexagonal and  $150^\circ$  cone angle axicon array showing the capability of imaging and simultaneous generation of multiple Bessel beams.

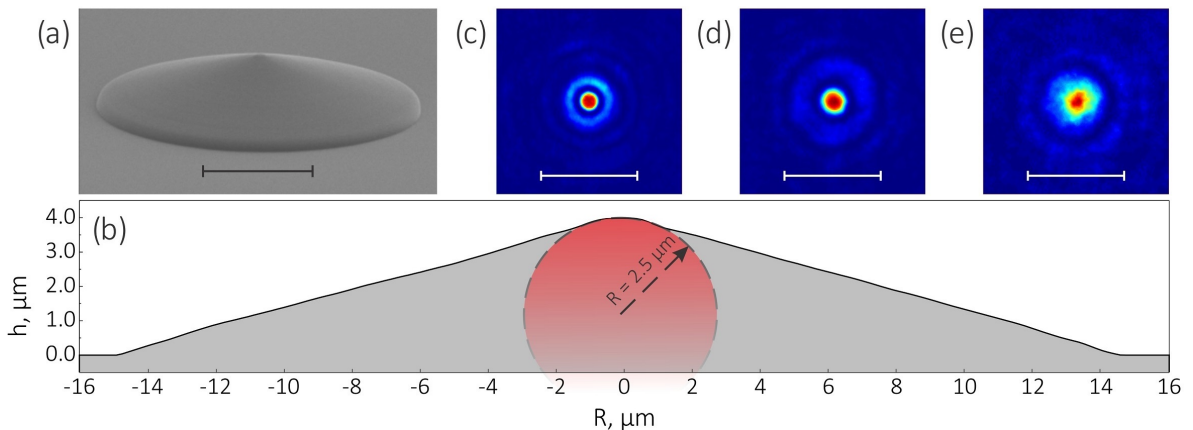


**Fig. 4.1:** (a) SEM image of the conical microlens under  $75^\circ$  viewing angle with cone angle of  $150^\circ$  and (b) experimental cross-section profile of the same microlens showing the curvature radius of the tip. Radial intensity profiles of a generated Bessel beam as a function of the conical lens cone angle: (c)  $150^\circ$ , (d)  $160^\circ$  and (e)  $170^\circ$ . Scale bar in (a), (c)–(e) images:  $10\ \mu\text{m}$ .

### 4.3 Spiral phase plates

A spiral phase plate (SPP) is an optical element whose complex transmittance has a linear phase dependence with respect to azimuthal angle  $\varphi$ . The light beam passed through the SPP undergoes a phase-change and is transformed into the beam containing optical vortex. Such beams refer to light field endowed with on-axis phase singularity, which corresponds to a local azimuthal phase dependence of the electric field of the form  $\exp(il\varphi)$  where  $l$  is called the topological charge. Optical vortices carry non-zero orbital angular momentum and have many applications [75–77]. Among all possible techniques to generate vortex beams [78–81], the use of SPPs is distinguished by the highest efficiency. Here we show a fast and reliable direct laser writing of high precision SPP's with  $l = 1, 2, 3$  and 4 topological charge whose step height is defined as  $h = (l\lambda)/(n_p - n_a)$  with  $\lambda = 633$  nm,  $n_p = 1.504$  and  $n_a = 1$ . It is crucial to match SPP's step height to the integer value of  $l$  perfectly in order to retain the rotational symmetry of the optical vortex. In order to assess the step height of the produced  $l = 1$  SPP, we have measured it at five different places with the optical profilometer. The obtained results are shown in Fig. 4.2 (a). It shows that the average step height coincides well with the designed value:  $h_e = 1.240 \pm 0.019$   $\mu\text{m}$  and  $h_t = 1.256$   $\mu\text{m}$ , respectively. Then, the optical performance of the fabricated vortex generators were evaluated. The calculated and observed far field intensity patterns obtained from SPP with  $R = 40$   $\mu\text{m}$  and  $l = 1$  are shown in Fig. 4.2 (b) and (c) in the case of  $\omega_0/R = 1/2$ . In agreement with main features of vortex beams we observe a doughnut intensity pattern. In contrast, a complex intensity pattern is observed when  $\omega_0/R = 2$  (Fig. 4.2 (d) and (e)). In that case the on-axis intensity is non-zero and the rotation symmetry is broken. This can be explained as the result of interference between the field diffracted by the inner and the outer part of the illuminated SPP. A spiraling intensity pattern with  $l$ -fold symmetry whose handedness depends on the sign of the topological charge is found. In conclusion, high fidelity DLW of microscopic SPPs with integer topological charge has been realized. Both the structure of the MOCs themselves and their use as vortex beam generators has been demonstrated.

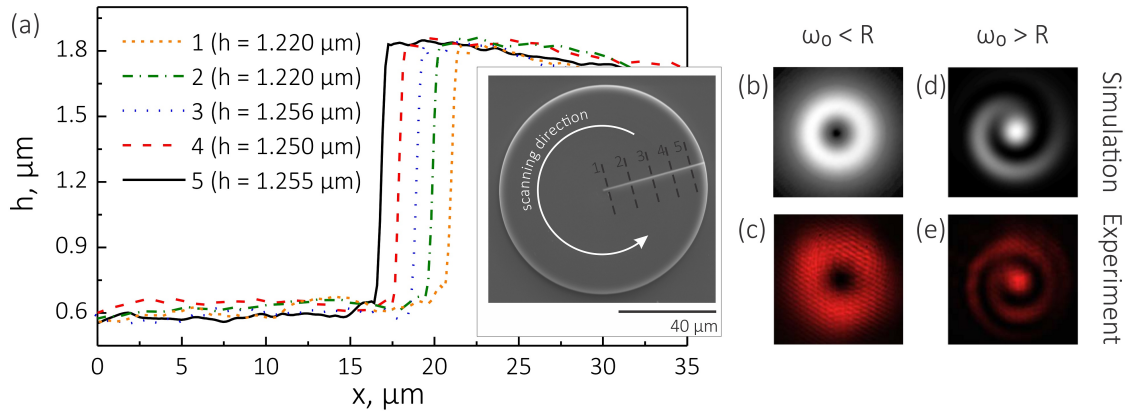


**Fig. 4.2:** (a) Step height dependence on the radius of the SPP, shown in the inset's SEM image. (b) – (e) Calculated and experimental data of the SPP's optical characterization. Far (left row) and near (right row) field intensity patterns when a focused Gaussian beam waist is normally incident onto a SPP. The data corresponds to  $\omega_0/R = 1/2$  and  $\omega_0/R = 2$ .

#### 4.4 Bifunctional optical elements

The generation of vortex beams at the micron scale out of usual Gaussian beams has been restricted so far to the case of Laguerre-Gauss-like (LG) diffracting fields. In contrast, in this section we consider the realization of MOCs that enable the generation of higher-order Bessel-Gauss-like (HOBG) beams, hence pseudo-nondiffracting optical vortex beams. By doing so, we aim at merging the field of singular integrated optics with that of nondiffracting light fields. This is done by combining SPPs, which transform Gaussian beams into LG-like beams, and axicons, which transform LG beams into HOBG-like beams. The proposed geometry of the monolithic MOC (helical axicon) structure is made of an axicon and a SPP sharing a common basis and suspended on micropillars. The helical axicon is described by two independent parameters: (1) the step height  $h$  of the SPP which is related to the topological charge  $l$ , and (2) the inclination angle  $\psi$  of the axicon which is related to the opening angle of the Bessel beam cone. Two sets of microstructures have been fabricated: (1)  $l = 1$  with  $\psi = 5^\circ, 10^\circ$ , and  $15^\circ$  and (2)  $\psi = 10^\circ$  with  $l = 1, 2$ , and  $3$ . A SEM image of a  $100 \mu\text{m}$  diameter structure is shown in Fig. 4.3 (a) in the case  $l = 1$  and  $\psi = 15^\circ$ , which qualitatively confirms the overall quality of the fabricated element. Then, the optical performance was evaluated. The dependence of the azimuthally averaged intensity profiles as a function of propagation distance is shown in Fig. 4.3 (b) next to simulation (c). The agreement between the experimental data and simulations is fairly good. We observe the on-axis line of darkness that is characteristic to the presence of an optical vortex. This is illustrated in Fig. 4.3 (d), where radial intensity profile is shown for  $l = 1$  and  $\psi = 10^\circ$ . The topological charge of the phase singularity can be determined from Fig. 4.3 (e), where the characteristic „forked” intensity pattern associated with the  $2l\pi$  circulation of the optical phase is seen. Moreover, we can observe an abrupt phase shift of  $\pi$  for the field at radial distances that correspond to null intensity values, which is reminiscent of the Bessel beams. To conclude, we have shown that DLW can be used to realize photopolymerized monolithic singular MOCs for the generation of pseudo-nondiffracting HOBG beams.

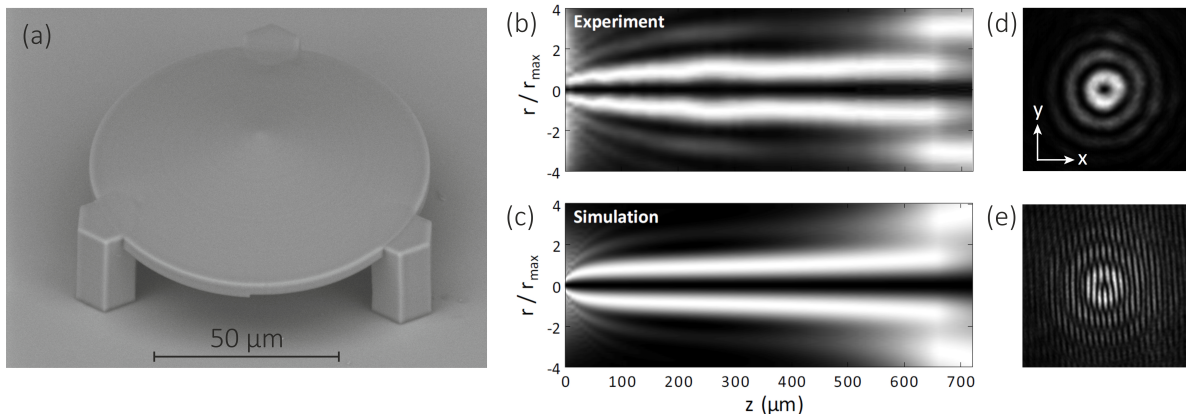


**Fig. 4.3:** (a) SEM image of a fabricated monolithic microstructure with  $50 \mu\text{m}$  radius,  $l = 1$  and  $\psi = 15^\circ$ . (b) Experimental data and (c) simulations of radial intensity profile as a function of the propagation distance for  $l = 1$  and  $\psi = 5^\circ$ . (d) and (e) characterization of higher-order Bessel beams for  $l = 1$  and  $\psi = 10^\circ$ . (d) Intensity profile, (e) interference pattern exhibiting the typical fork pattern.

### 4.5 Fabrication of complex microoptical elements on fiber tip

The last section of this chapter is devoted to the fabrication of the MOCs on the fiber tip and solving the critical technical issue – accurate centering of the MOC according to the fiber core, which can limit the performance efficiency of the whole optical system. The MOC’s centering accuracy can be defined as the ratio of the MOC’s deviation from the fiber and mode field’s diameter at the end of the fiber:  $\phi = [\Delta d / (2\omega_0)] \times 100$ . Thereby, the centering error can be reduced by either improving the sample positioning, thus reducing  $\Delta d$ , or by increasing the mode field diameter  $2\omega_0$ . The latter method is more desirable in practice and it will be presented in this section. This is demonstrated by the fabrication of a hybrid MOC consisting of a conical lens, an aspherical lens, and three pillars. The structure is designed to modify the Gaussian output of the fiber into Bessel beam. The pillars serve two purposes: (1) to ensure the attachment of the free-form MOC to the fiber, and (2) to control the free-space between the fiber and the hybrid MOC and, consequently, the mode diameter which increases due to diffraction phenomena. The purpose of the aspherical and conical microlenses is to ensure the collimation of the Gaussian beam and the generation of a Bessel beam, respectively. Firstly, the dimensions of the aspherical and conical lenses should be determined. It is done in accordance with the measured properties of the light beam which is emerging from the end of the single mode optical fiber (Fig. 4.4, first row of data). Next, the aspherical lens is fabricated on the fiber tip to verify the effect of Gaussian beam collimation (Fig. 4.4, second row of data). The obtained results show that after 50  $\mu\text{m}$  traveling, the beam waist increases by 2.21  $\mu\text{m}$ , corresponding to 4 %. According to this, the hybrid

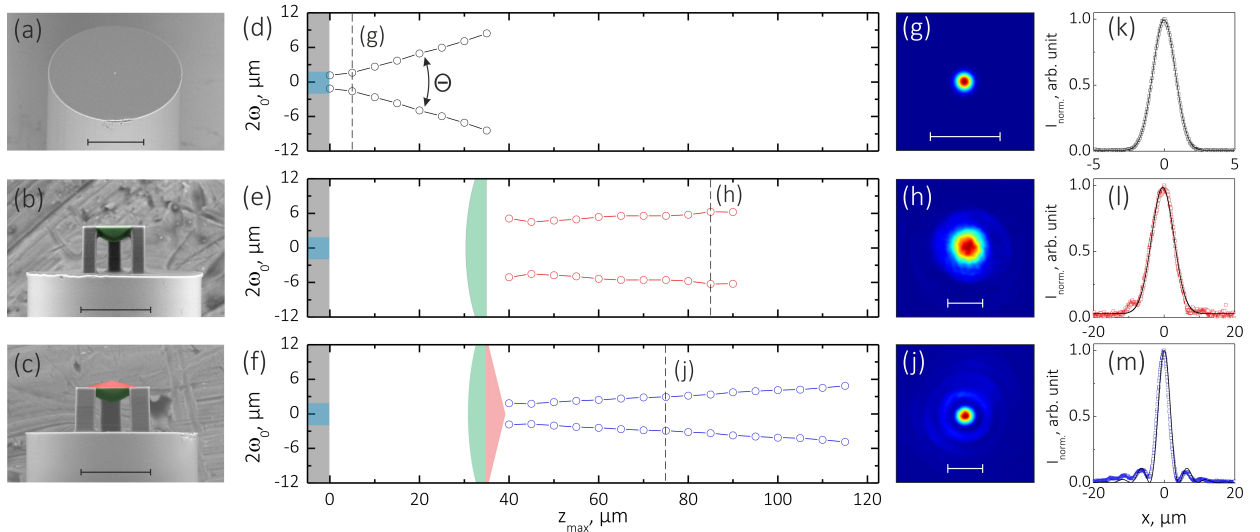


**Fig. 4.4:** SEM images of the cleaved single mode optical fiber (a), aspherical lens (b) and hybrid microoptical element (c) fabricated on the tip of the fiber. Beam waist dependence on the propagation distance from the fiber tip through the fiber (d), aspherical lens (e) and hybrid MOC fabricated on the fiber tip. 2D intensity profiles and transverse distributions of the propagating fiber mode ((g) and (k)), collimated Gaussian ((h) and (l)) and Bessel ((j) and (m)) beams measured along dashed lines in (d) – (f) images. Scale bars in (a) – (c) images: 50  $\mu\text{m}$ , in (g) – (j) images: 10  $\mu\text{m}$ .

MOC was fabricated on the fiber tip and the optical performance of the system was characterized (Fig. 4.4, third row of data). Even though the waist diameter increases by  $5.32\ \mu\text{m}$  after  $75\ \mu\text{m}$  propagation distance, we have observed the generation of a Bessel beam. In addition, we experimentally demonstrate the increase of propagation distance of a Bessel beam 5 times in comparison to the case when the axicon of the same parameters would be fabricated directly on the fiber tip. Finally, let us evaluate the influence of the beam expansion to the reduction of the centering problem. It was found that  $\Delta d = 600\ \text{nm}$ ,  $2\omega_0 = 2.26\ \mu\text{m}$  and  $2\omega = 16.76\ \mu\text{m}$  according to measured experimental results (here  $2\omega_0$  and  $2\omega$  are the beam waist at the end-face of the fiber and at  $35\ \mu\text{m}$  distance from the fiber, respectively). Subsequently,  $\Delta d/(2\omega_0)$  equals to  $\phi_0 = 27\ \%$  and  $\phi_0 = 4\ \%$ , respectively. The beam expansion, therefore, reduces the relative off-axis error 7-fold.

In conclusion, we have proposed a new method to overcome the problem of accurate centering of the microoptical components fabricated using direct laser writing on the tip of a single mode optical fiber by employing mode field expansion.

---

## Optical Components with Gradient Refractive Index

---

*Material related to this chapter was published in [A8] and presented at [C16] conference.*

In the previous chapter it was demonstrated that propagation of the light beams at the micrometer scale can be controlled via free-form microoptical elements due to the sophisticated surface profile fabricated by DLW technique. It is well known that propagation of the light can be controlled with gradient-index elements (GRIN) which refer to structures endowed with the gradual variation of the refractive index. Commonly, GRIN elements are manufactured using well-known methods: chemical vapor deposition [82], ion exchange [83], neutron irradiation [84], thermal [85], UV [86] and diffusion-assisted lithography [87]. However, all of them lack the possibility to embody arbitrary shape components, except for a very recent study [88]. On the other hand, the DLW technique is distinguished by the unique feature of fabricating complex shape 3D structures, but the possibility to manufacture structures with the imprinted spatial refractive index distribution have not been reported so far. Before moving onto the results' section we want to mention that refractive index of the fabricated microstructures depends on their chemical properties – degree of conversion (the percentage of consumed C=C bonds during the polymerization process). Therefore, this chapter begins with the analysis of the chemical properties using Raman microspectroscopy technique and in the second part we will come back to GRIN microoptics.

### 5.1 Change in chemical properties under light exposure

For the determination of interplay between the DLW exposure conditions and the degree of conversion (DC) of fabricated microstructures, three sets of samples consisting of  $15 \times 15 \times 10 \mu\text{m}^3$  cuboids were prepared for the Raman microspectroscopy experiments. Each array was fabricated by varying the average power in the range of 20 – 220  $\mu\text{W}$  and the sample translation velocity from 0.05 mm/s to 5 mm/s. Fig. 5.1 (a) shows Raman spectra of the non-polymerized thin film of the prepolymer SZ2080. Three peaks situated at  $1593 \text{ cm}^{-1}$ ,  $1640 \text{ cm}^{-1}$  and  $1714 \text{ cm}^{-1}$  are seen. The first one is attributed to the aromatic ring vibrations of the Irgacure 369 photoinitiator, the second – to the C=C stretching mode of the cross-linking methacrylate group



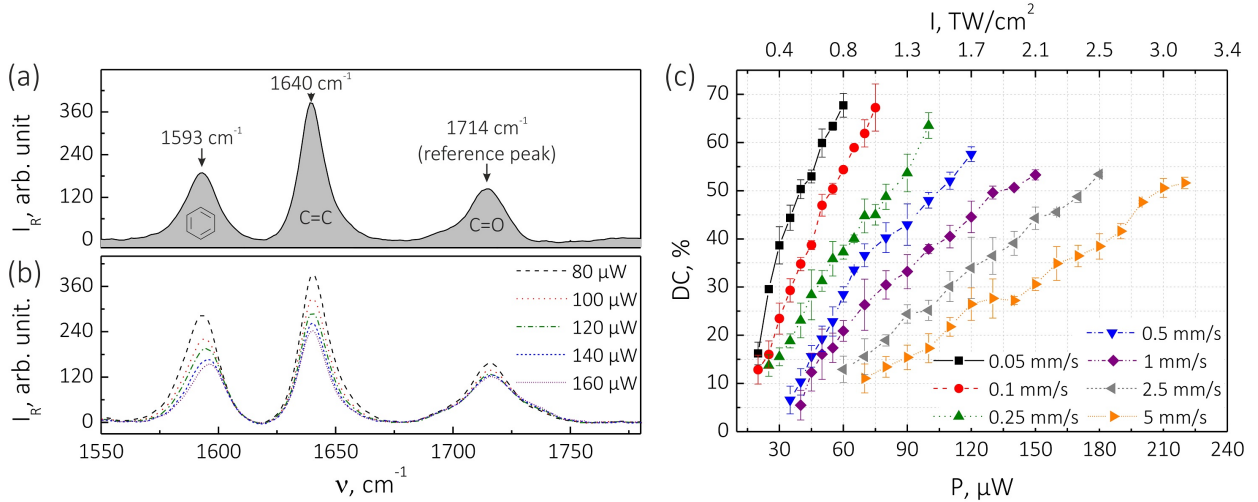


**Fig. 5.1:** (a) Raman spectra of the prepolymer and (b) evolution of the cuboids fabricated at 2.5 mm/s velocity. (c) Experimental data for the DC as a function of the DLW average laser power/intensity and scanning velocity.

and the third – to the stretching mode of the carbonyl group (C=O). The typical Raman spectra evolution of the cuboids photopolymerized with a varying average laser power at constant velocity is shown in Fig. 5.1 (b). The decrease of the C=C peak intensity with the increase of the laser beam power is clearly seen. It indicates consumption and conversion of C=C bonds into single C–C bonds in the methacrylic groups in the presence of light absorption. Meanwhile, the integrated intensity ( $S$ ) of the carbonyl group remains unaffected. Since this peak does not participate in the chain growth reactions, it was used as a reference for the calculation of DC.

The degree of conversion was calculated by comparing the methacrylate C=C stretching mode to a reference band C=O before ( $n$ ) and after ( $p$ ) photopolymerization [89]:

$$DC = \left[ 1 - \left( \frac{S_p(\text{C=C})/S_p(\text{C=O})}{S_n(\text{C=C})/S_n(\text{C=O})} \right) \right] \times 100. \quad (5.1)$$

It should be noted that prior to determination of DC, the fluorescence background was photo-bleached maintaining two crucial conditions: (1) no arising or disappearance of the peaks was observed and (2) the ratio of the peak intensity was constant with the applied pretreatment exposure time. In Fig. 5.1 (c) we plot mean values of the DC as a function of the average power and velocity. A rapid increase in the DC with the increase in laser power is observed. Meanwhile, the decrease in the DC from  $\approx 68\%$  to  $\approx 52\%$  with the increase in the writing velocity from 0.05 mm/s to 5 mm/s is found. Also, the achieved maximum value of the DC is in close agreement with previously published results [90, 91]. To summarize, the highest DC can be achieved in two ways:  $P \rightarrow \max$  when  $v = \text{const}$  and  $v \rightarrow \min$  when  $P = \text{const}$ .

## 5.2 Tailoring of the refractive index

In the following, based on the Raman microspectroscopy findings, we examine optical properties of the photopolymerized SZ2080. We decided to evaluate the refractive index of the fabricated prisms at the case corresponding to  $\Delta DC \approx 45\%$  at  $P = 40 \mu\text{W}$ . The refractive index was measured with a Michelson interferometer according to the setup described in Chapter 2. Since the intensity of the light field is related to its phase ( $\varphi$ ), the refractive index change in respect to air ( $n_{air} = 1$ ) can be evaluated as follows:

$$\Delta n = \frac{\varphi \lambda}{2\pi h}, \quad (5.2)$$

where  $h$  is the height of the prism and  $\varphi$  – phase shift. The obtained results are summarized in Table 5.1. It can be seen that it is possible to achieve refractive index change in the SZ2080 polymer up to  $\Delta n = n_1 - n_5 = (1.16 \pm 0.12) \times 10^{-2}$  depending on the DLW conditions, i.e. exposure dosage. Moreover, a positive correlation between the degree of conversion and refractive index exists. The higher the DC, the more strongly the cross-linked network of monomers is polymerized corresponding to the increase in the refractive index.

The GRIN element was designed and fabricated with consideration of the refractive index measurements (Fig. 5.2 (a)). The element is fabricated in a „zig-zag” recording manner with the increase in exposure dosage towards the structure’s center and the decrease towards the opposite edge in the horizontal direction ( $x$  axis), while the exposure dosage is constant in the perpendicular direction ( $y$  axis). It reveals that the lens is a flat-top element in both directions even if the exposure dosage varies continuously in the  $x$  axis. This ensures that the change in optical properties of the fabricated component is not caused by its surface shape.

Finally, we measured the refractive index of the GRIN element along the  $x$  and  $y$  axes employing the aforementioned interferometric technique. Quantitative analysis of the refractive index distribution along both axes is shown in Fig. 5.2 (b). Obviously, as was intended, the refractive index varies continuously in the  $x$  direction, but is uniform in the  $y$  direction. Also, the index distribution obtained along the  $x$  axis is distinguished by the symmetry within the error bars and can be expressed as:

**Table 5.1:** Experimentally measured DC and RI of the trapezoidal prisms fabricated at  $40 \mu\text{W}$  power and alternating velocity corresponding to accumulated energy dosage:  $D_{acc.} = D_p \times N_p$ , here  $D_p$  is the energy dosage per pulse and  $N_p$  – number of pulses.

No.	$v$ , mm/s	$D_{acc.}$ , J/cm <sup>2</sup>	DC, %	$n$
$n_1$	0.05	304	$50.3 \pm 2.0$	$1.5112 \pm 0.0010$
$n_2$	0.1	152	$34.8 \pm 1.4$	$1.5099 \pm 0.0010$
$n_3$	0.25	61	$23.1 \pm 3.6$	$1.5061 \pm 0.0015$
$n_4$	0.5	30	$10.4 \pm 2.7$	$1.5046 \pm 0.0011$
$n_5$	1	15	$5.5 \pm 3.1$	$1.4996 \pm 0.0012$

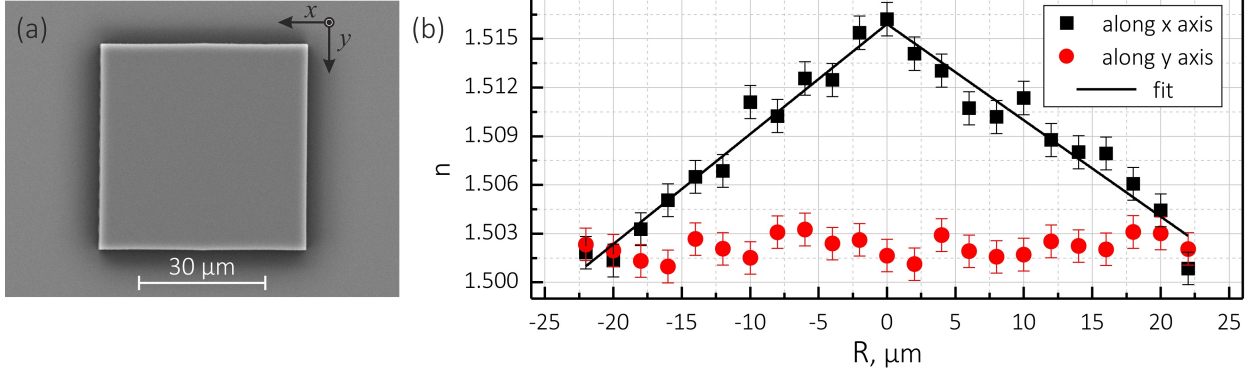


**Fig. 5.2:** (a) Top view SEM image of the polymerized GRIN structure and (b) the measured refractive index profile of it along  $x$  and  $y$  axes.

$n(x) = n_0 + k_1x$  for  $x < 0$  and  $n(x) = n_0 + k_2x$  for  $x > 0$ , where  $n_0 = 1.5159 \pm 0.0004$ ,  $k_1 = (6.78 \pm 0.37) \times 10^{-4}$  and  $k_2 = (-5.93 \pm 0.37) \times 10^{-4}$ . Thus, the attained results prove that the fabricated microstructure is indeed a GRIN element.

To conclude, we have investigated the interplay between the degree of conversion and the refractive index of microstructures fabricated at various DLW experimental parameters. Based on the Raman microspectroscopy results, we have found that the degree of conversion is within a 6–70 % range and increases with the applied DLW exposure dosage. Also, we have achieved refractive index change in the SZ2080 material up to  $\Delta n = (1.54 \pm 0.11) \times 10^{-2}$ . Moreover, we reveal the linear dependence among processing parameters (average laser power and scanning velocity) providing handbook knowledge. Finally, we have demonstrated that DLW technology due to its point-by-point scanning nature can be used for the manufacturing of GRIN microoptics by precisely controlling the refractive index. This could find applications in anamorphic light beam shaping, where aberration-free and plane optical surface components are desirable.

---

## Conclusions

---

First statement to defend is supported by these conclusions:

1. Laser-induced damage experiments of hybrid polymer SZ2080 conducted with Nd:YAG and Yb:KGW laser systems revealed that its optical resistance is in the range of tens  $\text{J}/\text{cm}^2$  at nanosecond pulse duration regime (1064 nm and 532 nm, 11 ns and 6.2 ns, 50 Hz) and varies in 0.1–0.6  $\text{J}/\text{cm}^2$  range at femtosecond pulse duration regime (1030 nm and 515 nm, 343 fs, 50 kHz).
2. Study of the photoinitiator's effect to the optical resistance of the SZ2080 polymer at multi-shot (S-on-1) regime showed that it has no considerable influence at the fundamental harmonic (1064 nm and 1030 nm) both at nano- and femtosecond pulse duration cases. Meanwhile, at the second harmonic (532 nm and 515 nm) it was found that laser-induced damage threshold decreases ten times from 13.67  $\text{J}/\text{cm}^2$  to 1.44  $\text{J}/\text{cm}^2$  at nanosecond pulse duration regime and two times from 0.13  $\text{J}/\text{cm}^2$  to 0.06  $\text{J}/\text{cm}^2$  at femtosecond pulse duration regime. Such trends are explained by the reduction of energy difference between the ground and the lowest excited states determined by the effect of conjugation of a photoinitiator.
3. The results obtained at nanosecond pulse duration regime indicate that optical resistance of the saturated polymers (SZ2080, PDMS and PMMA) is higher than that of conjugated polymers (SU-8 and OrmoComp). At femtosecond pulse duration regime and second harmonic (515 nm), damage threshold directly depends on the  $\Delta E$  energy. An increase of the damage threshold value from  $\approx 0.65 \text{ J}/\text{cm}^2$  to  $\approx 0.9 \text{ J}/\text{cm}^2$  can be observed at the point where three instead of two photons are required for the absorption.

Second statement to defend is supported by these conclusions:

4. Using direct laser writing system, consisting of Yb:KGW laser source (300 fs, 515 nm, 200 kHz), linear air bearing stages and galvanometric scanner, and applying concentric ring and spiral scanning algorithms with 0.1–0.5  $\text{TW}/\text{cm}^2$  laser intensity, the singular optical elements and their arrays were fabricated at the micrometer scale:
  - a) conical lenses and arrays thereof with the following parameters: 30  $\mu\text{m}$  diameter,  $5^\circ$ ,  $10^\circ$  and  $15^\circ$  inclination angle, 2.5  $\mu\text{m}$  tip radius of curvature and 100 % fill factor;

- 
- b) spiral phase plates which are 80  $\mu\text{m}$  in diameter and have a topological charge of 1, 2, 3 and 4 order;
  - c) monolithic bifunctional elements which are 100  $\mu\text{m}$  in diameter and consist of  $5^\circ$ ,  $10^\circ$  or  $15^\circ$  inclination angle conical lenses and 1, 2 or 3 order topological charge spiral phase plates;
  - d) hybrid components, consisting of  $15^\circ$  inclination angle conical lens and 40  $\mu\text{m}$  diameter aspheric lens, integrated onto the single mode fiber tip in order to optimize the manufacturing process.
5. Investigation of the amplitude and phase properties of the He-Ne laser beam, propagating through the aforementioned elements, revealed that these beams have properties of the optical vortexes and zero and first order Gaussian and Bessel beams: invariability under propagation, phase singularity, annular intensity distribution,  $\pi$  phase shift between adjacent rings, zero intensity at the central part of the beam, the dependence of the propagation distance and central core spot size of the beam on the inclination angle of the conical lenses. The experimental data are supported by the numerical simulations.

Third statement to defend is supported by these conclusions:

6. Based on the Raman microspectroscopy results, we have found that the degree of conversion of microstructures fabricated at various DLW experimental parameters (average laser power in the range of 20–220  $\mu\text{W}$  and scanning velocity – 0.05–5 mm/s) is within a 6–68 % range and directly depends on the exposure dosage of the laser irradiation as a 3rd degree function of the average laser power:  $D \propto P^3t$ .
7. It was determined that the refractive index of the microstructures, corresponding to 6–50 % degree of conversion values and produced via DLW technique, is different and can acquire up to  $\Delta n = (1.16 \pm 0.12) \times 10^{-2}$  change depending on DLW processing parameters. It indicates that refractive index of the fabricated microstructures is directly linked to the number of consumed C=C chemical bonds during polymerization reaction.
8. For the first time, it was demonstrated that DLW technology can be used for the manufacturing of gradient refractive index microoptical elements out of hybrid prepolymer SZ2080 by varying the exposure within 14–304 J/cm<sup>2</sup> range and resulting in refractive index change up to  $\Delta n = (1.54 \pm 0.11) \times 10^{-2}$ .

---

## Bibliography

---

- [1] O. Homburg, D. Hauschild, and V. Lissotschenko, Manufacturing and application of micro-optics, *Optik & Photonik* **3** (4), 48–52 (2008).
- [2] S. Maruo, O. Nakamura, and S. Kawata, Three-dimensional microfabrication with two-photon-absorbed photopolymerization, *Opt. Lett.* **22** (2), 132 (1997).
- [3] R. Guo, S. Xiao, X. Zhai, J. Li, A. Xia, and W. Huang, Micro lens fabrication by means of femtosecond two photon photopolymerization, *Opt. Express* **14** (2), 810–816 (2006).
- [4] S. Sinzinger and J. Jahns, *Microoptics*, 2nd ed. (Wiley–VCH, 2003).
- [5] H. Zappe, *Fundamentals of micro-optics*, 1st ed. (Cambridge University Press, 2010).
- [6] K. Iga, Y. Kokobun, and M. Oikawa, *Fundamentals of microoptics*, 1st ed. (New York Academic Press, 1984).
- [7] R. Hooke, *Micrographia: some physiological descriptions of minute bodies by magnifying glasses*, 1st ed. (London: J. Martyn and J. Allestry, 1665).
- [8] L. d’Auria, J. Huignard, A. Roy, and E. Spitz, Photolithographic fabrication of thin film lenses, *Opt. Commun.* **5** (4), 232–235 (1972).
- [9] T. Fujita, H. Nishihara, and J. Koyama, Fabrication of micro lenses using electron-beam lithography, *Opt. Lett.* **6** (12), 613 (1981).
- [10] K. Iga, M. Oikawa, S. Misawa, J. Banno, and Y. Kokubun, Stacked planar optics: an application of the planar microlens, *Appl. Opt.* **21** (19), 3456 (1982).
- [11] D. Daly, R. F. Stevens, M. C. Hutley, and N. Davies, The manufacture of microlenses by melting photoresist, *J. Meas. Sci. Technol.* **1** (8), 759–766 (1990).
- [12] R. Voelkel, Micro-optics: From high-end to mass-market, *Optik & Photonik* **4** (4), 36–40 (2009).
- [13] R. Voelkel, Wafer-scale micro-optics fabrication, *Adv. Opt. Techn.* **1** (3) (2012).
- [14] B. Kress and P. Meyrueis, *Applied digital optics: from micro-optics to nanophotonics*, 1st ed. (John Wiley & Sons, Ltd, 2009).
- [15] M. B. Stern, Fabricating binary optics: Process variables critical to optical efficiency, *J. Vac. Sci. Technol. B* **9** (6), 3117 (1991).
- [16] Y. Oppliger, P. Sixt, J. Stauffer, J. Mayor, P. Regnault, and G. Voirin, One-step 3D shaping using a gray-tone mask for optical and microelectronic applications, *Microelectron. Eng.* **23** (1-4), 449–454 (1994).
- [17] T. Fujita, H. Nishihara, and J. Koyama, Blazed gratings and fresnel lenses fabricated by electron-beam lithography, *Opt. Lett.* **7** (12), 578 (1982).
- [18] M. T. Gale, Fabrication of continuous-relief micro-optical elements by direct laser writing in photoresists, *Opt. Eng.* **33** (11), 3556 (1994).
- [19] N. K. Sheridan, Production of blazed gratings, *Appl. Phys. Lett.* **12** (9), 316 (1968).
- [20] S. Biehl, R. Danzebrink, P. Oliveira, and M. Aegerter, *J. Sol-Gel Sci. Technol.* **13** (1/3), 177–182 (1998).

- [21] <http://luxexcel.com/.net>.
- [22] G. Hatakoshi, M. Kawachi, K. Terashima, Y. Uematsu, A. Amano, and K. Ueda, Grating axicon for collimating Čerenkov radiation waves, *Opt. Lett.* **15** (23), 1336–1338 (1990).
- [23] H. M. Phillips, Excimer-laser-produced nanostructures in polymers, *Opt. Eng.* **32** (10), 2424 (1993).
- [24] L. R. Harriott, R. E. Scotti, K. D. Cummings, and A. F. Ambrose, Micromachining of integrated optical structures, *Appl. Phys. Lett.* **48** (25), 1704 (1986).
- [25] C. N. LaFratta, J. T. Fourkas, T. Baldacchini, and R. A. Farrer, Multiphoton fabrication, *Angew. Chem. Int. Ed.* **46** (33), 6238–6258 (2007).
- [26] S. Maruo and J. Fourkas, Recent progress in multiphoton microfabrication, *Laser Photonics Rev.* **2** (1-2), 100–111 (2008).
- [27] K.-S. Lee, R. H. Kim, D.-Y. Yang, and S. H. Park, Advances in 3D nano/microfabrication using two-photon initiated polymerization, *Prog. Polym. Sci.* **33** (6), 631–681 (2008).
- [28] S.-H. Park, D.-Y. Yang, and K.-S. Lee, Two-photon stereolithography for realizing ultra-precise three-dimensional nano/microdevices, *Laser Photonics Rev.* **3** (1-2), 1–11 (2009).
- [29] M. Farsari and B. N. Chichkov, Materials processing: Two-photon fabrication, *Nature Photon.* **3** (8), 450–452 (2009).
- [30] G. von Freymann, A. Ledermann, M. Thiel, I. Staude, S. Essig, K. Busch, and M. Wegener, Three-dimensional nanostructures for photonics, *Adv. Funct. Mater.* **20** (7), 1038–1052 (2010).
- [31] Y.-L. Zhang, Q.-D. Chen, H. Xia, and H.-B. Sun, Designable 3D nanofabrication by femtosecond laser direct writing, *Nano Today* **5** (5), 435–448 (2010).
- [32] M. Malinauskas, M. Farsari, A. Piskarskas, and S. Juodkazis, Ultrafast laser nanostructuring of photopolymers: A decade of advances, *Phys. Rep.* **533** (1), 1–31 (2013).
- [33] X. Zhou, Y. Hou, and J. Lin, A review on the processing accuracy of two-photon polymerization, *AIP Advances* **5** (3), 030701 (2015).
- [34] Q.-D. Chen, D. Wu, L.-G. Niu, J. Wang, X.-F. Lin, H. Xia, and H.-B. Sun, Phase lenses and mirrors created by laser micronanofabrication via two-photon photopolymerization, *Appl. Phys. Lett.* **91** (17), 171105 (2007).
- [35] M. Malinauskas, H. Gilbergs, A. Žukauskas, V. Purlys, D. Paipulas, and R. Gadonas, A femtosecond laser-induced two-photon photopolymerization technique for structuring microlenses, *J. Opt.* **12** (3), 035204 (2010).
- [36] D. Wu, Q.-D. Chen, L.-G. Niu, J. Jiao, H. Xia, J.-F. Song, and H.-B. Sun, 100% fill-factor aspheric microlens arrays (AMLA) with sub-20-nm precision, *IEEE Photon. Technol. Lett.* **21** (20), 1535–1537 (2009).
- [37] Y. Li, Y. Yu, L. Guo, S. Wu, C. Chen, L. Niu, A. Li, and H. Yang, High efficiency multilevel phase-type fresnel zone plates produced by two-photon polymerization of SU-8, *J. Opt.* **12** (3), 035203 (2010).
- [38] X.-F. Lin, Q.-D. Chen, L.-G. Niu, T. Jiang, W.-Q. Wang, and H.-B. Sun, Mask-free production of integratable monolithic micro logarithmic axicon lenses, *J. Light. Tech.* **28** (8), 1256–1260 (2010).
- [39] J. K. Gansel, M. Latzel, A. Frolich, J. Kaschke, M. Thiel, and M. Wegener, Tapered gold-helix metamaterials as improved circular polarizers, *Appl. Phys. Lett.* **100** (10), 101109 (2012).
- [40] S. H. Park, S. H. Lee, D.-Y. Yang, H. J. Kong, and K.-S. Lee, Subregional slicing method to increase three-dimensional nanofabrication efficiency in two-photon polymerization, *Appl. Phys. Lett.* **87** (15), 154108 (2005).

- [41] J. Serbin, A. Egbert, A. Ostendorf, B. N. Chichkov, R. Houbertz, G. Domann, J. Schulz, C. Cronauer, L. Fröhlich, and M. Popall, Femtosecond laser-induced two-photon polymerization of inorganic organic hybrid materials for applications in photonics, *Opt. Lett.* **28** (5), 301–303 (2003).
- [42] D. Wu, S.-Z. Wu, L.-G. Niu, Q.-D. Chen, R. Wang, J.-F. Song, H.-H. Fang, and H.-B. Sun, High numerical aperture microlens arrays of close packing, *Appl. Phys. Lett.* **97** (3), 031109 (2010).
- [43] M. Malinauskas, A. Žukauskas, V. Purlys, K. Belazaras, A. Momot, D. Paipulas, R. Galdonas, A. Piskarskas, H. Gilbergs, and etal., Femtosecond laser polymerization of hybrid/integrated micro-optical elements and their characterization, *J. Opt.* **12** (12), 124010 (2010).
- [44] Y. Hu, Y. Chen, J. Ma, J. Li, W. Huang, and J. Chu, High-efficiency fabrication of aspheric microlens arrays by holographic femtosecond laser-induced photopolymerization, *App. Phys. Lett.* **103** (14), 141112 (2013).
- [45] L. Yang, A. El-Tamer, U. Hinze, J. Li, Y. Hu, W. Huang, J. Chu, and B. N. Chichkov, Parallel direct laser writing of micro-optical and photonic structures using spatial light modulator, *Opt. Laser. Eng.* **70**, 26–32 (2015).
- [46] Z. Li, J. Torgersen, A. Ajami, S. Mühleder, X. Qin, W. Husinsky, W. Holnthoner, A. Ovsianikov, J. Stampfl, and R. Liska, Initiation efficiency and cytotoxicity of novel water-soluble two-photon photoinitiators for direct 3D microfabrication of hydrogels, *RSC Adv.* **3** (36), 15939–15946 (2013).
- [47] T. Bückmann, N. Stenger, M. Kadic, J. Kaschke, A. Frölich, T. Kennerknecht, C. Eberl, M. Thiel, and M. Wegener, Tailored 3D mechanical metamaterials made by dip-in direct-laser-writing optical lithography, *Adv. Mater.* **24** (20), 2710–2714 (2012).
- [48] K. Obata, A. El-Tamer, L. Koch, U. Hinze, and B. N. Chichkov, High-aspect 3D two-photon polymerization structuring with widened objective working range (WOW-2PP), *Light Sci. Appl.* **2** (12), e116 (2013).
- [49] Press release: <http://www.nanoscribe.de> .
- [50] V. Melissinaki, M. Farsari, and S. Pissadakis, A fiber-endface, fabry–perot vapor micro-sensor fabricated by multiphoton polymerization, *IEEE J. Sel. Top. Quantum.* **21** (4), 1–10 (2015).
- [51] Z. Xie, S. Feng, P. Wang, L. Zhang, X. Ren, L. Cui, T. Zhai, J. Chen, Y. Wang, X. Wang, and etal., Demonstration of a 3D radar-like SERS sensor micro- and nanofabricated on an optical fiber, *Adv. Opt. Mater.* (2015).
- [52] H. Wang, Z. Xie, M. Zhang, H. Cui, J. He, S. Feng, X. Wang, W. Sun, J. Ye, P. Han, and etal., A miniaturized optical fiber microphone with concentric nanorings grating and microsprints structured diaphragm, *Optics & Laser Technology* , JOLTD1500476 Aug (2015).
- [53] D. Wu, L.-G. Niu, S.-Z. Wu, J. Xu, K. Midorikawa, and K. Sugioka, Ship-in-a-bottle femtosecond laser integration of optofluidic microlens arrays with center-pass units enabling coupling-free parallel cell counting with a 100% success rate, *Lab Chip* **15** (6), 1515–1523 (2015).
- [54] I. Zinkiewicz, J. Haberko, and P. Wasylczyk, Highly asymmetric near infrared light transmission in an all-dielectric grating-on-mirror photonic structure, *Opt. Express* **23** (4), 4206 (2015).
- [55] M. Nawrot, I. Zinkiewicz, B. Włdarczyk, and P. Wasylczyk, Transmission phase gratings fabricated with direct laser writing as color filters in the visible, *Opt. Express* **21** (26), 31919 (2013).
- [56] L. Kuna, C. Sommer, F. Reil, J. R. Krenn, P. Hartmann, P. Pachler, H. Hoschopf, and F. P. Wenzl, Femtosecond laser processing as a versatile tool for advanced solid state



- lighting sources: From efficacy enhancement to colour temperature control, *Appl. Surf. Sci.* **258** (23), 9213–9217 (2012).
- [57] Q.-S. Li, L.-J. Wang, Z.-N. Tian, X.-F. Lin, T. Jiang, J. Zhang, X. Zhang, J.-H. Zhao, A.-W. Li, and L. Qin, Direct integration of aspherical microlens on vertical-cavity surface emitting laser emitting surface for beam shaping, *Opt. Commun.* **300**, 269–273 (2013).
- [58] A. Ovsianikov, J. Viertl, B. Chichkov, M. Oubaha, B. MacCraith, I. Sakellari, A. Giakoumaki, D. Gray, M. Vamvakaki, M. Farsari, and C. Fotakis, Ultra-low shrinkage hybrid photosensitive material for two-photon polymerization microfabrication, *ACS Nano* **2** (11), 2257–2262 (2008).
- [59] ISO 21254-2:2011. *Lasers and laser-related equipment-Test methods for laser-induced damage threshold-Part 2: Threshold determination*, (2011).
- [60] A. Melninkaitis, M. Ščiuka, G. Batavičiūtė, J. Mirauskas, S. Bucka, and V. Sirutkaitis, Automated test station for characterization of optical resistance with ultrashort pulses at multikilohertz repetition rates, *Proc. SPIE* **8530**, 85301M (2012).
- [61] G. Batavičiūtė, P. Grigas, L. Smalakys, and A. Melninkaitis, Revision of laser-induced damage threshold evaluation from damage probability data, *Rev. Sci. Instrum.* **84** (4), 045108 (2013).
- [62] J. Tauc, Optical properties and electronic structure of amorphous Ge and Si, *Mater. Res. Bull.* **3** (1), 37–46 (1968).
- [63] Q.-D. Chen, X.-F. Lin, L.-G. Niu, D. Wu, W.-Q. Wang, and H.-B. Sun, Dammann gratings as integratable micro-optical elements created by laser micromanufacturing via two-photon photopolymerization, *Opt. Lett.* **33** (21), 2559–2561 (2008).
- [64] E. Brasselet, M. Malinauskas, A. Žukauskas, and S. Juodkazis, Photopolymerized microscopic vortex beam generators: Precise delivery of optical orbital angular momentum, *Appl. Phys. Lett.* **97** (21), 211108 (2010).
- [65] M. D. Turner, M. Saba, Q. Zhang, B. P. Cumming, G. E. Schröder-Turk, and M. Gu, Miniature chiral beamsplitter based on gyroid photonic crystals, *Nature Photon* **7** (10), 801–805 (2013).
- [66] K. Takada, H.-B. Sun, and S. Kawata, Improved spatial resolution and surface roughness in photopolymerization-based laser nanowriting, *Appl. Phys. Lett.* **86** (7), 071122 (2005).
- [67] I. Sakellari, A. Gaidukeviciute, A. Giakoumaki, D. Gray, C. Fotakis, M. Farsari, M. Vamvakaki, C. Reinhardt, A. Ovsianikov, and B. N. Chichkov, Two-photon polymerization of titanium-containing sol-gel composites for three-dimensional structure fabrication, *Appl. Phys. A* **100** (2), 359–364 (2010).
- [68] Y. Jee, M. F. Becker, and R. M. Walser, Laser-induced damage on single-crystal metal surfaces, *J. Opt. Soc. Am. B* **5** (3), 648–659 (1988).
- [69] C. W. Carr, H. B. Radousky, and S. G. Demos, Wavelength dependence of laser-induced damage: Determining the damage initiation mechanisms, *Phys. Rev. Lett.* **91** (12), 127402 (2003).
- [70] M. Jupe, L. Jensen, K. Starke, D. Ristau, A. Melninkaitis, R. Grigonis, and V. Sirutkaitis, Quantized behavior of fs-LIDT in dielectric layers, *Proc. SPIE* **5647** (2005).
- [71] A. Chmel, Fatigue laser-induced damage in transparent materials, *Mat. Sci. Eng. B* **49** (3), 175–190 (1997).
- [72] R. Srinivasan, E. Sutcliffe, and B. Braren, Ablation and etching of polymethylmethacrylate by very short (160 fs) ultraviolet (308 nm) laser pulses, *Appl. Phys. Lett.* **51** (16), 1285 (1987).
- [73] R. J. DeVoe, H. W. Kalweit, C. A. Leatherdale, and T. R. Williams, Voxel shapes in two-photon microfabrication, *Proc. SPIE* **4797**, 310–316 (2003).

- 
- [74] O. Brzobohatý, T. Čižmár, and P. Zemánek, High quality quasi-Bessel beam generated by round-tip axicon, *Opt. Express* **16** (17), 12688–12700 (2008).
- [75] H. He, M. E. J. Friese, N. R. Heckenberg, and H. Rubinsztein-Dunlop, Direct observation of transfer of angular momentum to absorptive particles from a laser beam with a phase singularity, *Phys. Rev. Lett.* **75** (5), 826–829 (1995).
- [76] M. Prasciolu, F. Tamburini, G. Anzolin, E. Mari, M. Melli, A. Carpentiero, C. Barbieri, and F. Romanato, Fabrication of a three-dimensional optical vortices phase mask for astronomy by means of electron-beam lithography, *Microelectron. Eng.* **86** (4-6), 1103–1106 (2009).
- [77] D. Wildanger, J. Bückers, V. Westphal, S. W. Hell, and L. Kastrup, A sted microscope aligned by design, *Opt. Express* **17** (18), 16100–16110 (2009).
- [78] M. Beijersbergen, R. Coerwinkel, M. Kristensen, and J. Woerdman, Helical-wavefront laser beams produced with a spiral phaseplate, *Opt. Commun.* **112** (5-6), 321–327 (1994).
- [79] M. Harris, C. Hill, and J. Vaughan, Optical helices and spiral interference fringes, *Opt. Commun.* **106** (4-6), 161–166 (1994).
- [80] M. Beresna, M. Gecevičius, P. G. Kazansky, and T. Gertus, Radially polarized optical vortex converter created by femtosecond laser nanostructuring of glass, *Appl. Phys. Lett.* **98** (20), 201101 (2011).
- [81] H. Lin and M. Gu, Creation of diffraction-limited non-Airy multifocal arrays using a spatially shifted vortex beam, *Appl. Phys. Lett.* **102** (8), 084103 (2013).
- [82] M. A. Pickering, R. L. Taylor, and D. T. Moore, Gradient infrared optical material prepared by a chemical vapor deposition process, *Appl. Opt.* **25** (19), 3364–3372 (1986).
- [83] S. Ohmi, H. Sakai, Y. Asahara, S. Nakayama, Y. Yoneda, and T. Izumitani, Gradient-index rod lens made by a double ion-exchange process, *Appl. Opt.* **27** (3), 496–499 (1988).
- [84] P. Sinai, Correction of optical aberrations by neutron irradiation, *Appl. Opt.* **10** (1), 99–104 (1971).
- [85] J.-H. Liu, P.-C. Yang, and Y.-H. Chiu, Fabrication of high-performance, gradient-refractive-index plastic rods with surfmer-cluster-stabilized nanoparticles, *J. Polym. Sci. A Polym. Chem.* **44** (20), 5933–5942 (2006).
- [86] J.-H. Liu and Y.-H. Chiu, Process equipped with a sloped UV lamp for the fabrication of gradient-refractive-index lenses, *Opt. Lett.* **34** (9), 1393–1395 (2009).
- [87] C. Ye and R. R. McLeod, Grin lens and lens array fabrication with diffusion-driven photopolymer, *Opt. Lett.* **33** (22), 2575–2577 (2008).
- [88] A. C. Urness, K. Anderson, C. Ye, W. L. Wilson, and R. R. McLeod, Arbitrary grin component fabrication in optically driven diffusive photopolymers, *Opt. Express* **23** (1), 264–273 (2015).
- [89] L. E. Silva Soares, A. A. Martin, and A. L. Barbosa Pinheiro, Degree of conversion of composite resin: A Raman study, *J. Clin. Laser Med. Surg.* **21** (6), 357–362 (2003).
- [90] K. Cicha, Z. Li, K. Stadlmann, A. Ovsianikov, R. Markut-Kohl, R. Liska, and J. Stampfl, Evaluation of 3D structures fabricated with two-photon-photopolymerization by using FTIR spectroscopy, *Appl. Phys.* **110** (6), 064911 (2011).
- [91] F. Burmeister, S. Steenhusen, R. Houbertz, U. D. Zeitner, S. Nolte, and A. Tünnermann, Materials and technologies for fabrication of three-dimensional microstructures with sub-100 nm feature sizes by two-photon polymerization, *Laser Appl.* **24** (4), 042014 (2012).

---

## Santrauka

---

### OPTINIŲ ELEMENTŲ ŠVIESOS VALDYMUI MIKROMETRINIAME MASTELYJE FORMAVIMAS TIESIOGINIO LAZERINIO RAŠYMO BŪDU

Mikrooptiniai komponentai – tai yra optiniai elementai, kurių geometriniai matmenys siekia nuo kelių mikrometrų iki vieno milimetro. Jų gamybai nuo pat 1980 metų yra naudojamos įvairios technologijos, kurios skirstomos į tris plačias grupes: 1) fotolitografijos, 2) savaiminio formavimo ir 3) atimamojo pobūdžio metodus. Tačiau pastaruoju laikotarpiu vykstantys spartūs mikrominiatūrizacijos ir funkcijų išplėtimo procesai reikalauja inovatyvių komponentų, gebančių tiksliai valdyti šviesos sklaidimą mikrometriniame mastelyje. Anksčiau minėtos tradicinės technologijos pasiekia savo galimybių ribas ir ne visas idėjas galima įgyvendinti. Tai skatina esamų technologijų vystymą ir naujų kūrimą. Viena iš tokių – 1997 metais pademonstruotas tiesioginis lazerinis rašymas šviesai jautriose medžiagose (polimeruose). Ši technologija išsiskiria iš kitų gamybos metodų unikalia galimybe vieno proceso metu formuoti įvairios geometrinės formos trimačius darinius su submikrometrine erdvine raiška. Praėjus devyneriems metams nuo pirmųjų darbų, ši technologija buvo panaudota ir mikrooptinių elementų formavimui. Šiuo darbu plėtojame tiesioginio lazerinio rašymo technologiją, demonstruodami jos tęstinumą ir naujas galimybes.

Šios disertacijos tikslas – eksperimentiškai ištirti galimybę tiesioginio lazerinio rašymo technologija iš hibridinio polimero formuoti singuliarios ir trūkios geometrinės formos bei gradientinio lūžio rodiklio pasiskirstymo optinius elementus ir panaudoti juos šviesos valdymui mikrometriniame mastelyje. Taip pat charakterizuoti formavimui naudojamą polimerinę medžiagą optiniais ir cheminiais aspektais.

Pirmajame rezultatų aptarimo skyriuje lazerio indukuoto pažeidimo metodika buvo tyrinėjamas tiesioginio lazerinio rašymo technologijoje naudojamų įvairių polimerų atsparumas optinei spinduliuotei. Naudojant Nd:YAG ir Yb:KGV lazerines sistemas ištirta pažeidimo slenksčio priklausomybė nuo lazerio impulso trukmės, bangos ilgio ir impulsų skaičiaus. Nustatyta, kad nanosekundžių trukmės impulsų atveju polimerų optinis atsparumas siekia iki poros dešimčių  $J/cm^2$ . O femtosekundžių trukmės impulsų atveju, polimerų pažeidimo slenkstis sumažėja viena arba dviem eilėmis ir įgyja vertes 0,1 – 0,6  $J/cm^2$  intervale.

Antrajame rezultatų aptarimo skyriuje apžvelgiami mikrooptinių elementų formavimo principai ir nagrinėjama eksperimentinių sąlygų įtaka šių komponentų geometrinės formos atitikimui modeliams. Remiantis gautais rezultatais pademonstruojama, kad tiesioginio lazerinio rašymo metodu galima formuoti įvairaus pagrindo kampo kūginius lęšius, nuo 1 iki 4 topologinio krūvio spiralines fazines plokšteles

---

ir sudėtinius monolitinius pastarųjų elementų junginius. Eksperimentinių rezultatų patikimumas patvirtintas tiriant šviesos sklaidimo ypatybes pro suformuotus komponentus. Nustatyta, kad šie šviesos pluoštai pasižymi optinių sūkurių bei nulinės ir aukštesnės eilės Gauso ir Beselio pluoštų savybėmis.

Trečiajame rezultatų aptarimo skyriuje Ramano mikrospektroskopijos ir interferenciniais metodais buvo tyrinėjamos iš hibridinio polimero SZ2080 suformuotų darinių cheminės ir optinės savybės bei jų tarpusavio ryšys. Empiriškai ištirta monomerų konversijos ir lūžio rodiklio priklausomybė nuo tiesioginio lazerinio rašymo eksperimentinių sąlygų. Nustatyta, kad monomerų konversija kinta nuo 6 % iki 68 %, o indukuojamas lūžio rodiklio pokytis gali siekti iki  $\Delta n = (1,16 \pm 0,12) \times 10^{-2}$ . Taip pat nustatyta, kad lūžio rodiklio pokytis tiesiogiai priklauso nuo polimerizacijos reakcijos metu sueikvojamų C=C jungčių. Tai sudarė sąlygas pirmą kartą pademonstruoti, kad tiesioginio lazerinio rašymo technologija galima formuoti tiksliai derinamo lūžio rodiklio pasiskirstymo elementus.

Šio disertacijos rezultatai atskleidžia, kad tiek tiesioginio lazerinio rašymo technologija, tiek ir joje naudojamos polimerinės medžiagos, yra tinkamos singuliaros geometrinės formos ir gradientinio lūžio rodiklio mikrooptinių elementų gamybai. Pademonstruojama, kad pastarieji elementai yra funkcionalūs ir gali būti panaudoti šviesos valdymui mikrometriniame mastelyje.

---

## Curriculum vitae

---

### Personal information

Name, Surname Albertas Žukauskas  
Address M. Marcinkevičiaus 15 – 4, Vilnius  
E-mail albertaszukauskas@gmail.com  
Place of birth Molėtai, Lithuania  
Date of birth February 24, 1986

### Education

Date 2009 09 – 2011 06  
Qualification Master of Science in Physics (Magna cum laude)  
Institution Vilnius University, Faculty of Physics  
Date 2005 09 – 2009 06  
Qualification Bachelor of Science in Physics  
Institution Vilnius University, Faculty of Physics  
Date 2003 09 – 2005 06  
Qualification Secondary Education  
Institution Molėtai gymnasium  
Date 1993 09 – 2009 06  
Qualification Lower Secondary Education  
Institution Molėtai Lower Secondary School

### Work experience

2011 05 – present VU LTC (junior research fellow)  
2010 09 – 2011 02 VU LTC (engineer)  
2009 04 – 2010 04 VU LTC (laboratory assistant)

### Internships

2010 04 – 2010 08 Hannover Laser Zentrum (Germany)  
2011 02 – 2011 04 Hannover Laser Zentrum (Germany)  
2011 09 14 – 17 Summer school “Photonics meets Biology” (Greece)  
2012 05 06 – 27 IESL–FORTH Research Institute (Greece)  
2013 02 08 – 03 29 Swinburne University of Technology (Australia)

---

## **Additional information**

Scholarships Memorial scholarship of prof. M. Yčas

Awards „Student Award” for poster presentation in the conference „Lasers and Optical Nonlinearity” (2013, Vilnius, Lithuania)

„Best Student Paper Award” in the conference SPIE „Photonics Europe” (2012, Brussels, Belgium)

„Young Scientist Award” for poster presentation in the conference „AMT-13” (2011, Palanga, Lithuania)